Novel role of Rac-Mid1 signaling in medial cerebellar development

Nakamura, Takashi ; Ueyama, Takehiko ; Ninoyu, Yuzuru ; Sakaguchi, Hirofumi ; Choijookhuu, Narantsog ; Hishikawa, Yoshitaka ; Kiyonari,…

(Citation)
Development,144(10):1863-1875

(Issue Date)
2017-05-15

(Resource Type)
journal article

(Version)
Version of Record

© 2017. Published by The Company of Biologists Ltd | Development (2017) 144, 1863-1875 doi:10.1242/dev.147900

RESEARCH ARTICLE

Novel role of Rac-Mid1 signaling in medial cerebellar development

Takashi Nakamura[1,2,*], Takehiko Ueyama[1,*,‡], Yuzuru Ninoyu[1], Hirofumi Sakaguchi[2], Narantsog Choijookhuu[3], Yoshitaka Hishikawa[3], Hiroshi Kiyonari[4], Masaaki Kohta[5], Mizuho Sakahara[6], Ivan de Curtis[7], Eiji Kohmura[5], Yasuo Hisa[2], Atsu Aiba[6,8] and Naoaki Saito[1,‡]

ABSTRACT

Rac signaling impacts a relatively large number of downstream targets; however, few studies have established an association between Rac pathways and pathological conditions. In the present study, we generated mice with double knockout of *Rac1* and *Rac3* (*Atoh1-Cre;Rac1*$^{flox/flox}$*;Rac3*$^{-/-}$) in cerebellar granule neurons (CGNs). We observed impaired tangential migration at E16.5, as well as numerous apoptotic CGNs at the deepest layer of the external granule layer (EGL) in the medial cerebellum of *Atoh1-Cre;Rac1*$^{flox/flox}$*;Rac3*$^{-/-}$ mice at P8. *Atoh1-Cre;Rac1*$^{flox/flox}$*;Rac3*$^{-/-}$ CGNs differentiated normally until expression of p27^{kip1} and NeuN in the deep EGL at P5. Primary CGNs and cerebellar microexplants from *Atoh1-Cre;Rac1*$^{flox/flox}$*;Rac3*$^{-/-}$ mice exhibited impaired neuritogenesis, which was more apparent in Map2-positive dendrites. Such findings suggest that impaired tangential migration and final differentiation of CGNs have resulted in decreased cerebellum size and agenesis of the medial internal granule layer, respectively. Furthermore, Rac depleted/deleted cells exhibited decreased levels of Mid1 and impaired mTORC1 signaling. *Mid1* depletion in CGNs produced mild impairments in neuritogenesis and reductions in mTORC1 signaling. Thus, a novel Rac-signaling pathway (Rac1-Mid1-mTORC1) may be involved in medial cerebellar development.

KEY WORDS: Cerebellum, Cerebellar granule neurons, Midline 1, mTORC1, Opitz G/BBB syndrome, Rac

INTRODUCTION

During brain development, migration of immature neurons from germinal zones to their final destination is essential for the establishment of proper circuitry. Two types of neuronal migration – tangential and radial – are required, and radial migration may occur in both inward and outward directions during cerebellar development (Chédotal, 2010; Wang and Zoghbi, 2001). Cerebellar granule neuron (CGN) progenitors are derived at E13-16 from the upper rhombic lip (RL), which is the primary germinal zone of CGNs. Beginning at E13, these progenitor cells migrate tangentially to form the surface of the cerebellar primordium: the external granule layer (EGL), which is the secondary germinal zone of CGNs. After proliferation in the EGL, CGN progenitors begin to differentiate and migrate to deeper layers. Subsequently, CGNs develop inward dendritic processes for radial migration (Kawaji et al., 2004). Inward radial migration, which is completed by P20 in mice (Hatten et al., 1997), is a major characteristic of cerebellar development. By contrast, Purkinje cells (PCs) migrate outwardly from the ventricular zone.

Rac (Rac1-3) is a member of the Rho family of small GTPases and plays important roles in neuritogenesis, including axonogenesis and dendritogenesis, neuronal migration and modulation of gene transcription (Bosco et al., 2009; Funahashi et al., 2014; Govek et al., 2005). Previous studies had shown that, although conditional *Rac1* knockout (KO) in telencephalon-derived neurons produced mild impairments in radial migration and axon guidance (Chen et al., 2007; Kassai et al., 2008), these phenotypes were apparently milder than those observed in studies using an electroporated dominant-negative *Rac1* mutant (Kawauchi et al., 2003). *Rac1*-KO mice generated using a Nestin-Cre system exhibited impaired radial migration and axonogenesis in CGNs (Tahirovic et al., 2010). Furthermore, although a relatively large number of downstream molecules and putative disease-related pathways have been suggested to involve Rac signaling, the number of diseases in which involvement of Rac-associated molecules/pathways has been established is quite low (Govek et al., 2005; Stankiewicz and Linseman, 2014).

Midline 1 (*MID1*) is the gene responsible for Opitz G/BBB syndrome (OS), which is characterized by malformations that affect midline structures, such as laryngotracheoesophageal, cardiac and urogenital abnormalities. Mid1 is a microtubule-associated E3 ubiquitin ligase (Schweiger and Schneider, 2003) that regulates the degradation of the catalytic subunit of protein phosphatase 2A (Ppp2ca) via interaction with the α4 subunit of Pp2a (Trockenbacher et al., 2001). One-third of individuals with OS also exhibit developmental defects of the CNS, which mainly consist of hypoplasia/agenesis of the medial cerebellum (Fontanella et al., 2008; Pinson et al., 2004); however, clinical manifestations of OS in the CNS, as well as in the body, show variable expressivity. Indeed, although *Mid1*-KO mice have been reported to show hypoplasia of the anterior portion of the medial cerebellum, no other abnormalities were observed (Lancioni et al., 2010). Furthermore, no correlation between the position of the mutation in *MID1* and clinical phenotypes of OS has been reported (Fontanella et al., 2008). Thus, the underlying pathogenesis of OS remains to be fully elucidated.

Here, we have investigated the association between downstream targets of Rac and developmental abnormalities using mice with double KO (DKO) of *Rac1* and *Rac3* in CGNs (*Atoh1-Cre;Rac1*$^{flox/flox}$*;Rac3*$^{-/-}$). Impaired final differentiation with dendritogenesis of CGNs resulted in agenesis of the medial internal granule layer (IGL) due to disruptions in the radial

[1]Laboratory of Molecular Pharmacology, Biosignal Research Center, Kobe University, Kobe 657-8501, Japan. [2]Department of Otolaryngology-Head and Neck Surgery, Kyoto Prefectural University of Medicine, Kyoto 602-8566, Japan. [3]Division of Histochemistry and Cell Biology, Department of Anatomy, Faculty of Medicine, University of Miyazaki, Miyazaki 889-1692, Japan. [4]Animal Resource Development Unit and Genetic Engineering Team, RIKEN Center for Life Science Technologies, Kobe 650-0047, Japan. [5]Department of Neurosurgery, Kobe University Graduate School of Medicine, Kobe 650-0017, Japan. [6]Department of Molecular Genetics, Kobe University Graduate School of Medicine, Kobe 650-0017, Japan. [7]Division of Neuroscience, San Raffaele Scientific Institute, Milano 20132, Italy. [8]Laboratory of Animal Resources, Center for Disease Biology and Integrative Medicine, Graduate School of Medicine, The University of Tokyo, Tokyo 113-0033, Japan.
*These authors contributed equally to this work

‡Authors for correspondence (tueyama@kobe-u.ac.jp; naosaito@kobe-u.ac.jp)

T.U., 0000-0002-5647-3937

Received 7 December 2016; Accepted 31 March 2017

Development (2017) 144, 1863-1875 doi:10.1242/dev.147900

migration of CGNs. Furthermore, our findings suggest that Mid1 is a novel and transcriptionally regulated Rac target, and that Rac1-Mid1-mTORC1 signaling may be involved in producing agenesis of the medial IGL of *Atoh1-Cre;Rac1*$^{flox/flox}$*;Rac3*$^{-/-}$ cerebellum.

RESULTS

Rac1 and *Rac3* expression in CGNs during development of the IGL

To study the role of Rac GTPases in CGNs, we examined mRNA expression of *Rac1* (widely expressed) and *Rac3* (neuron specific) in the cerebellum using *in situ* hybridization. At P6, which is when CGNs begin to migrate radially to form the IGL (Hatten et al., 1997), *Rac1* and *Rac3* mRNAs were expressed almost exclusively in the EGL (Fig. 1A), where almost all cells are CGNs. At P21, patterns of *Rac1* and *Rac3* expression became PC dominant, particularly those of *Rac3* (Fig. 1B). Slender cells in the molecular layer (ML), which are implicated in the radial migration of CGNs, were *Rac1* positive (Fig. S1A). Although a previous study reported an absence of *Rac3* expression in the cerebellum (Tahirovic et al., 2010), our results suggested that both *Rac1* and *Rac3* are expressed in the developing CGNs and that *Rac1* expression is more dominant than that of *Rac3* (Fig. S1B).

Further deletion of *Rac3* in CGNs exacerbates the phenotype of *Rac1* KO: agenesis of the IGL in the anterior medial cerebellum of *Rac1*/*Rac3*-DKO mice

We generated *Rac1*-KO mice using *Atoh1-Cre* mice and *Rac1*$^{flox/flox}$ mice, hereafter referred to as *Atoh1-Cre;Rac1*$^{flox/flox}$ mice. Atoh1 is a transcription factor that is essential for the genesis of CGNs (Ben-Arie et al., 1997). Atoh1-positive cells emerge as early as E9.5 in the RL (Akazawa et al., 1995), and Atoh1-positive CGN progenitors migrate from the RL to form the EGL between E12.5 and E16.5 (Wang et al., 2005). The pattern of *Atoh1-Cre*-driven recombination was assessed using *Atoh1-Cre;tdTomato* mice. Consistent with the findings of previous reports, tdTomato fluorescence was observed in the developing EGL at the surface of the primordial cerebellum of *Atoh1-Cre;tdTomato* mice at E16.5, in the EGL at P0, and in both the EGL and IGL at P9. However, no such findings were observed in control mice (*CAG-Stop*^{flox}*-tdTomato*) (Fig. 2A). Although *Nestin-Cre;Rac1*$^{flox/flox}$ mice, in which the *Nestin* promoter functions in the cerebellum from E15.5 as well as in all neuronal progenitors in the cerebrum around E10.5 (Graus-Porta et al., 2001), were reported to exhibit poor balance (Tahirovic et al., 2010), we detected no obvious behavioral phenotype in *Atoh1-Cre;Rac1*$^{flox/flox}$ mice. Therefore, we generated DKO mice of *Rac1* and *Rac3* (*Atoh1-Cre;Rac1*$^{flox/flox}$*;Rac3*$^{-/-}$) by crossing *Atoh1-Cre;Rac1*$^{flox/flox}$ mice with *Rac3*-null mice, which have been reported to show normal microscopic development of the brain (Corbetta et al., 2005). *Atoh1-Cre;Rac1*$^{flox/flox}$*;Rac3*$^{-/-}$ mice exhibited severe ataxic gait when they began walking, and the phenotype was retained throughout life (Movie 1).

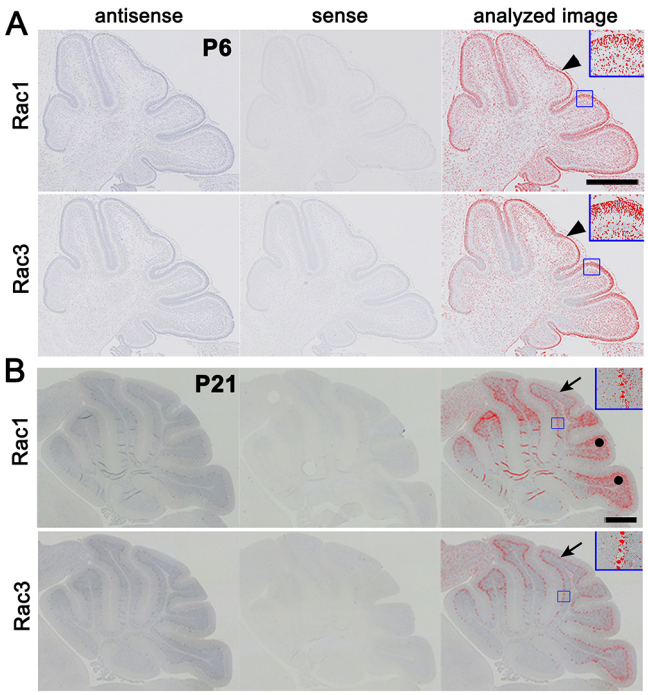

Fig. 1. *Rac1* and *Rac3* mRNA expression in CGNs during cerebellar development. (A,B) Sagittal sections of the cerebellum were obtained from P6 (A) and P21 (B) wild-type mice. *In situ* hybridization of *Rac1* (upper panels) and *Rac3* (lower panels) was performed using antisense (left panels) and sense (middle panels) DNA probes labeled with digoxigenin-11-dUTP. The right panels show the relative *Rac1* and *Rac3* mRNA signal levels determined using a digital image analyzer (red was assigned to positive). External granule layer: arrowheads. Purkinje cell layer: arrows. Circles indicate the internal granule layer. Insets are magnified images of the areas indicated by rectangles. Scale bars: 500 µm. $n \geq 4$ for each group.

Nissl-stained coronal sections of the cerebellum from 9-week-old *Atoh1-Cre;Rac1*$^{flox/flox}$*;Rac3*$^{-/-}$ mice exhibited agenesis of the medial IGL (Fig. 2B). *Rac1*$^{flox/flox}$*;Rac3*$^{-/-}$ (*Rac3* KO) mice and *Atoh1-Cre;Rac1*$^{flox/+}$*;Rac3*$^{-/-}$ mice had normal cerebella compared with *Atoh1-Cre* mice (Fig. 2B). *Rac1*$^{flox/flox}$*;Rac3*$^{-/-}$ mice were subsequently used as controls, in addition to *Atoh1-Cre* mice and *Rac1*$^{flox/flox}$ mice. Stepwise exacerbation of hypoplasia of the medial IGL was observed in the cerebellum of *Atoh1-Cre;Rac1*$^{flox/flox}$ (*Rac1* KO) mice and *Atoh1-Cre;Rac1*$^{flox/flox}$*;Rac3*$^{-/-}$ (*Rac1/Rac3* DKO) mice following the additional deletion of *Rac3* (Fig. 2B). *Atoh1-Cre;Rac1*$^{flox/flox}$*;Rac3*$^{-/+}$ mice exhibited mild ataxic gait when they began to walk, although the phenotype of these mice was much milder than that of *Atoh1-Cre;Rac1*$^{flox/flox}$*;Rac3*$^{-/-}$ mice throughout life. The thicknesses of the medial IGL in the control, *Atoh1-Cre;Rac1*$^{flox/flox}$ and *Atoh1-Cre;Rac1*$^{flox/flox}$*;Rac3*$^{-/-}$ cerebella were 143.8±3.1, 40.0±2.2 and 7.5±2.7 µm, respectively (Fig. 2B). In the medial *Atoh1-Cre;Rac1*$^{flox/flox}$*;Rac3*$^{-/-}$ cerebellum, the ML, PCL and IGL could not be fully distinguished (Fig. 2B). The affected regions (ML, PCL and IGL) of *Atoh1-Cre;Rac1*$^{flox/flox}$*;Rac3*$^{-/+}$ and *Atoh1-Cre;Rac1*$^{flox/flox}$*;Rac3*$^{-/-}$ cerebella were occupied by multiple layers of lightly stained large cells and densely stained small cells (insets in Figs 2B and 3A,B), whereas *Atoh1-Cre;Rac1*$^{flox/flox}$ cerebellum exhibited an aligned PCL and thin IGL (insets of Fig. 2B). The lightly stained large cells and some of the densely stained small cells were confirmed as calbindin-positive PCs and tdTomato-positive CGNs, respectively, using 12-week-old *Atoh1-Cre;Rac1*$^{flox/flox}$*;Rac3*$^{-/-}$*;tdTomato* mice (Fig. S2).

We then aimed to determine the proportion of the IGL affected by DKO of *Rac1* and *Rac3* using Nissl-stained serial sagittal (Fig. 3A) and coronal sections (Fig. 3B) of cerebellar tissue from 8-week-old mice. The anterior medial region (anatomically almost identical to the anterior cerebellar lobe) of the IGL (e.g. I-VII folia in the sagittal section) was hypoplastic/aplastic in the *Atoh1-Cre;Rac1*$^{flox/flox}$*;Rac3*$^{-/-}$ cerebellum.

Apoptosis of *Rac1*/*Rac3*-DKO CGNs in the deep layer of the EGL

We investigated the developmental processes of the EGL and IGL in *Atoh1-Cre;Rac1*$^{flox/flox}$*;Rac3*$^{-/-}$ mice from P4 to P17, when

Development (2017) 144, 1863-1875 doi:10.1242/dev.147900

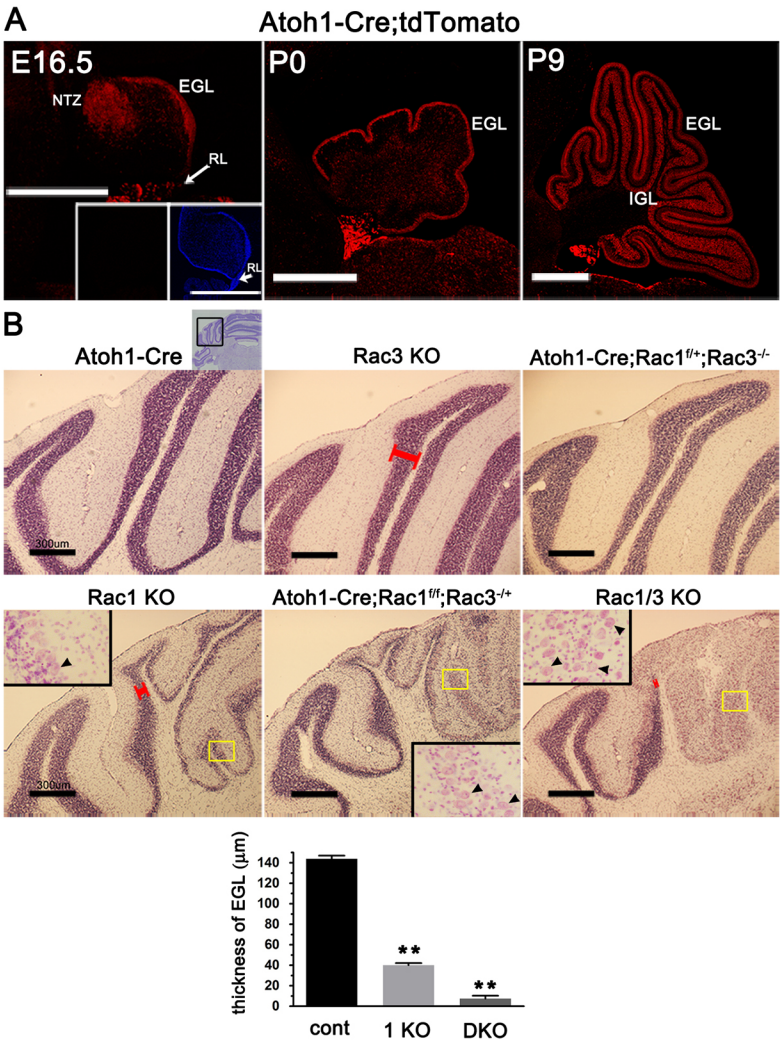

Fig. 2. Loss of the IGL by stepwise genetic deletion of *Rac* in CGNs using *Atoh1-Cre* mice. (A) Sagittal sections of the cerebellum were obtained from E16.5, P0 and P9 *Atoh1-Cre;tdTomato* mice and observed using an LSM 700 (Zeiss). Insets (left, tdTomato fluorescence; right, DAPI) in the E16.5 panel show the negative control obtained from *CAG-STOP^{flox}-tdTomato* mice. NTZ, nuclear transitory zone; RL, rhombic lip; EGL, external granule layer; IGL, internal granule layer. Scale bars: 500 µm. $n \geq 3$. (B) Coronal sections of the cerebellum were obtained from six mouse lines (9 weeks old) and stained using Nissl solution. The rectangle in the low-magnification image of the coronal section (upper left) indicates the location of the cerebellum photographed. Rectangular insets in the lower panels represent magnified images of the regions indicated by yellow rectangles in *Atoh1-Cre;Rac1$^{flox/flox}$* (*Rac1*-KO), *Atoh1-Cre;Rac1$^{flox/flox}$;Rac3$^{-/+}$* and *Atoh1-Cre;Rac1$^{flox/flox}$;Rac3$^{-/-}$* (*Rac1*/*Rac3*-DKO) cerebella. Arrowheads indicate lightly stained large cells. The thickness of the IGL is indicated by red lines (at the border of agenesis of the IGL in the *Rac1*/*Rac3*-DKO cerebellum and the corresponding position in the *Rac3*-KO (control) and *Rac1*-KO cerebella) was quantified (data are mean±s.e.m., $n \geq 5$, $^{**}P<0.01$ using Bonferroni's post-hoc test following one-way ANOVA). Scale bars: 300 µm.

proliferation of CGNs in the EGL and the subsequent formation of the IGL are robust (Hatten et al., 1997). At P4, coronal sections of the cerebellum from *Rac1$^{flox/flox}$;Rac3$^{-/-}$* mice and *Atoh1-Cre;Rac1$^{flox/flox}$;Rac3$^{-/-}$* mice showed comparable EGL thickness and lobular morphology (Fig. 4A). At P7, the *Atoh1-Cre;Rac1$^{flox/flox}$;Rac3$^{-/-}$* cerebellum was apparently smaller than the *Rac1$^{flox/flox}$;Rac3$^{-/-}$* cerebellum (Fig. 4A). Although the thickness of the EGL of the *Atoh1-Cre;Rac1$^{flox/flox}$;Rac3$^{-/-}$* cerebellum increased, the morphology of the EGL became abnormal, particularly in the medial cerebellum (Fig. 4A). At P10, the appearance of the IGL was abruptly absent in the medial *Atoh1-Cre;Rac1$^{flox/flox}$;Rac3$^{-/-}$* cerebellum, and this phenotype was retained at P17 in combination with the disappearance of the EGL (Fig. 4A).

To examine the mechanism of agenesis in the medial IGL of *Atoh1-Cre;Rac1$^{flox/flox}$;Rac3$^{-/-}$* mice between P7 and P10, we used active caspase 3 immunostaining to detect apoptotic cells. Many apoptotic cells were detected in the medial *Atoh1-Cre;Rac1$^{flox/flox}$;Rac3$^{-/-}$* cerebellum but not in the *Rac1$^{flox/flox}$;Rac3$^{-/-}$* cerebellum at P8 (Fig. 4B), whereas no apoptotic cells were detected in the *Atoh1-Rac1$^{flox/flox}$;Rac3$^{-/-}$* cerebellum at E16.5, P1 or P3. The number of apoptotic cells in the *Atoh1-Cre;Rac1$^{flox/flox}$;Rac3$^{-/+}$* cerebellum at P8 was ∼50% of that in the *Atoh1-Rac1$^{flox/flox}$;Rac3$^{-/-}$* cerebellum. Moreover, apoptotic cells were accumulated in the deep layer of the medial EGL of *Atoh1-Cre;Rac1$^{flox/flox}$;Rac3$^{-/-}$* mice (Fig. 4B).

To verify the mechanism underlying decreased cerebellum size in *Atoh1-Cre;Rac1$^{flox/flox}$;Rac3$^{-/-}$* mice relative to *Rac1$^{flox/flox}$;Rac3$^{-/-}$* mice, we examined sagittal sections of the cerebellum at E16.5. The distance from the RL to the most anterior point of the EGL, which is the longest path of tangential migration, was analyzed in four sections corresponding to those depicted in Fig. 3A; tangential migrations of *Atoh1-Cre;Rac1$^{flox/flox}$;Rac3$^{-/-}$* CGNs were significantly shorter than those of *Rac1$^{flox/flox}$;Rac3$^{-/-}$* CGNs in all four sections (Fig. 5). However, no significant difference in the thickness of the primordium of the EGL was observed between *Atoh1-Cre;Rac1$^{flox/flox}$;Rac3$^{-/-}$* and *Rac1$^{flox/flox}$;Rac3$^{-/-}$* mice for any of the four sections (Fig. 5). To further examine the proliferative capability of CGNs, we applied EdU pulse labeling to cerebellum at P4, when proliferation of CGNs is high (Hatten et al., 1997). No significant differences in EdU labeling index (ratio of Edu-positive cells/DAPI-positive cells) in the EGL were observed between *Atoh1-Cre;Rac1$^{flox/flox}$;Rac3$^{-/-}$* and *Rac1$^{flox/flox}$;Rac3$^{-/-}$* mice at 4 h after EdU injection (Fig. 6A,B). At 30 h after injection, EdU-labeled CGNs were observed throughout the EGL (Fig. 6A).

Thus, these results suggested that the smaller size of the *Atoh1-Cre;Rac1$^{flox/flox}$;Rac3$^{-/-}$* cerebellum is due to impaired tangential migration, and that agenesis of the IGL in the medial *Atoh1-Cre;Rac1$^{flox/flox}$;Rac3$^{-/-}$* cerebellum is caused by apoptosis in the EGL following normal proliferation of CGNs and development of the EGL.

Development (2017) 144, 1863-1875 doi:10.1242/dev.147900

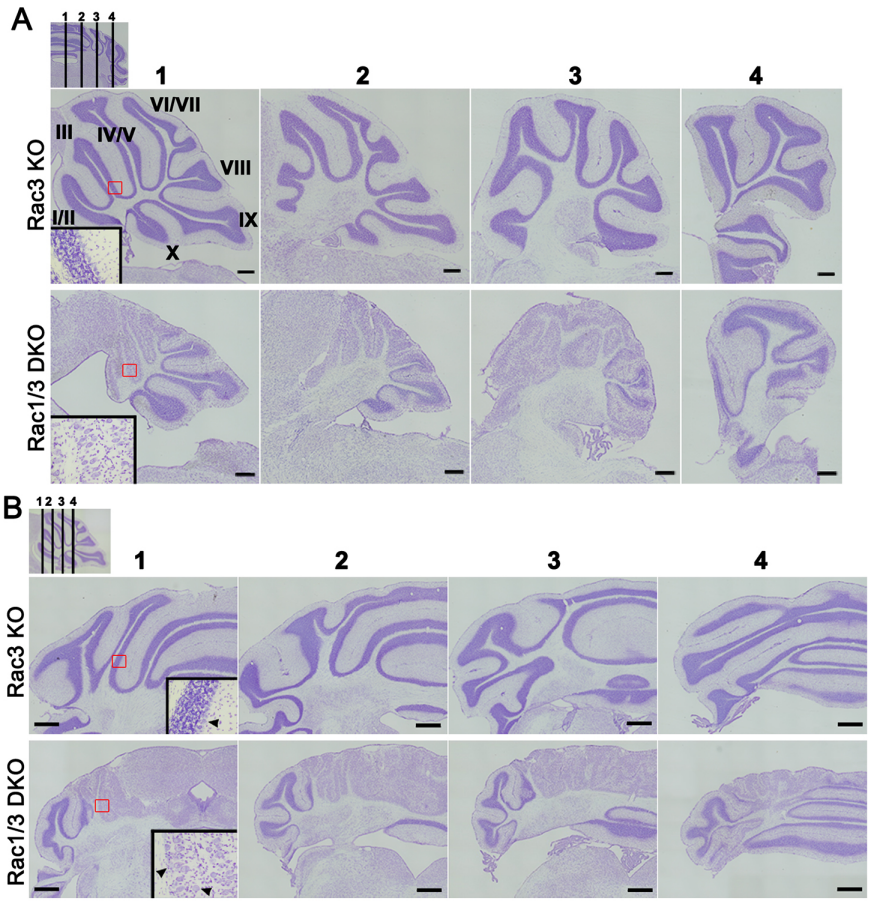

Fig. 3. Agenesis of the IGL of the anterior medial cerebellum in *Atoh1-Cre;Rac1*$^{flox/flox}$*;Rac3*$^{-/-}$ mice. (A,B) *Rac1*$^{flox/flox}$*;Rac3*$^{-/-}$ (*Rac3* KO=control) and *Atoh1-Cre;Rac1*$^{flox/flox}$*;Rac3*$^{-/-}$ (*Rac1*/*Rac3* DKO) mice were fixed at 8 weeks. Sagittal (A) and coronal (B) sections of the cerebellum were stained using Nissl solution. The locations photographed (1-4) are indicated by the lines in the low-magnification coronal section (upper left of A) and sagittal section (upper left of B). I-X in A indicate the lobules of the vermis. Rectangular insets in sagittal and coronal sections (location 1) represent magnified images of the regions indicated by red rectangles in *Rac3*-KO and *Rac1*/*Rac3*-DKO cerebellum. Arrowheads indicate lightly stained large cells. Scale bars: 250 µm in A; 500 µm in B. $n \geq 3$.

Rac1/*Rac3*-DKO CGNs differentiate to the final developmental stage

To examine differentiation capabilities of *Atoh1-Cre;Rac1*$^{flox/flox}$*;Rac3*$^{-/-}$ CGNs, we performed immunostaining using: Pax6, a marker for developing CGNs as well as CGNs in the IGL (Yamasaki et al., 2001); p27^{Kip1}, a marker for CGNs located in the deep region of the EGL (Mulherkar et al., 2014; Wang and Zoghbi, 2001); and NeuN, a marker for postmitotic CGNs (Mulherkar et al., 2014) at

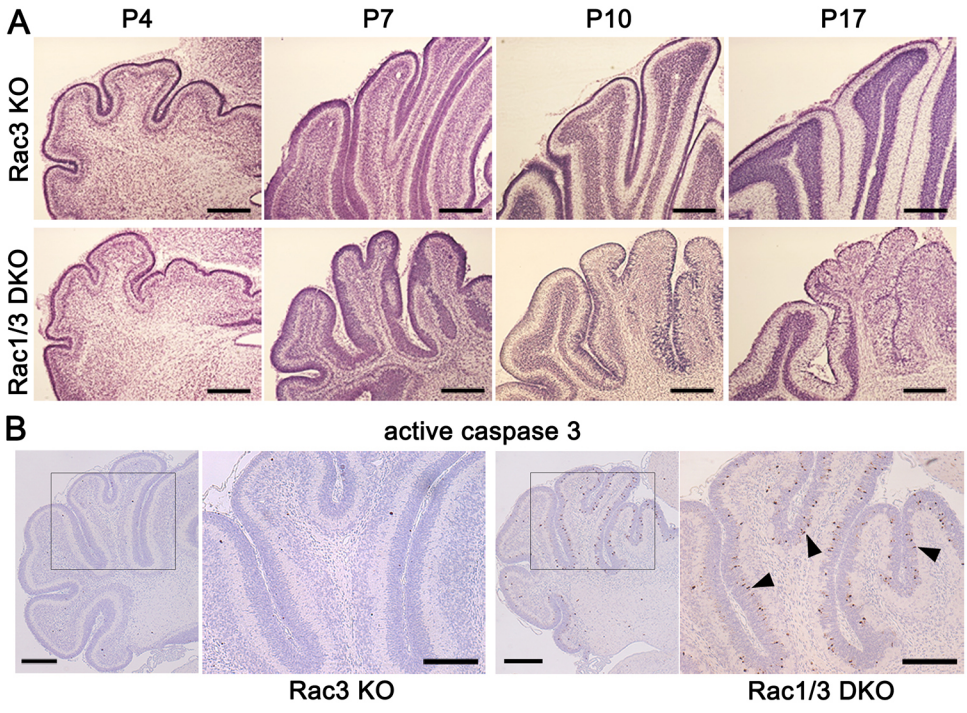

Fig. 4. Agenesis of the IGL in the *Atoh1-Cre;Rac1*$^{flox/flox}$*;Rac3*$^{-/-}$ cerebellum is caused by apoptosis in the deep layer of the EGL at P8. (A) Age-matched (P4-P17) tissue samples of the cerebellum from *Rac1*$^{flox/flox}$*;Rac3*$^{-/-}$ (*Rac3* KO) and *Atoh1-Cre;Rac1*$^{flox/flox}$*;Rac3*$^{-/-}$ (*Rac1*/*Rac3* DKO) mice were stained using Nissl solution. Coronal sections of the left *Rac1*/*Rac3*-DKO cerebellum show morphological abnormalities in the EGL from P7 and loss of the medial IGL from P10. Scale bars: 300 µm. $n \geq 3$. (B) Coronal sections of the left cerebellum at P8 were stained using an active caspase 3 antibody with Hematoxylin counterstaining. Apoptotic cells are detected in the deep layer of the medial EGL of *Rac1*/*Rac3*-DKO cerebellum and are indicated by arrowheads in the magnified image (scale bars: 100 µm) of the region indicated by the rectangle (scale bars: 300 µm). $n \geq 3$.

Development (2017) 144, 1863-1875 doi:10.1242/dev.147900

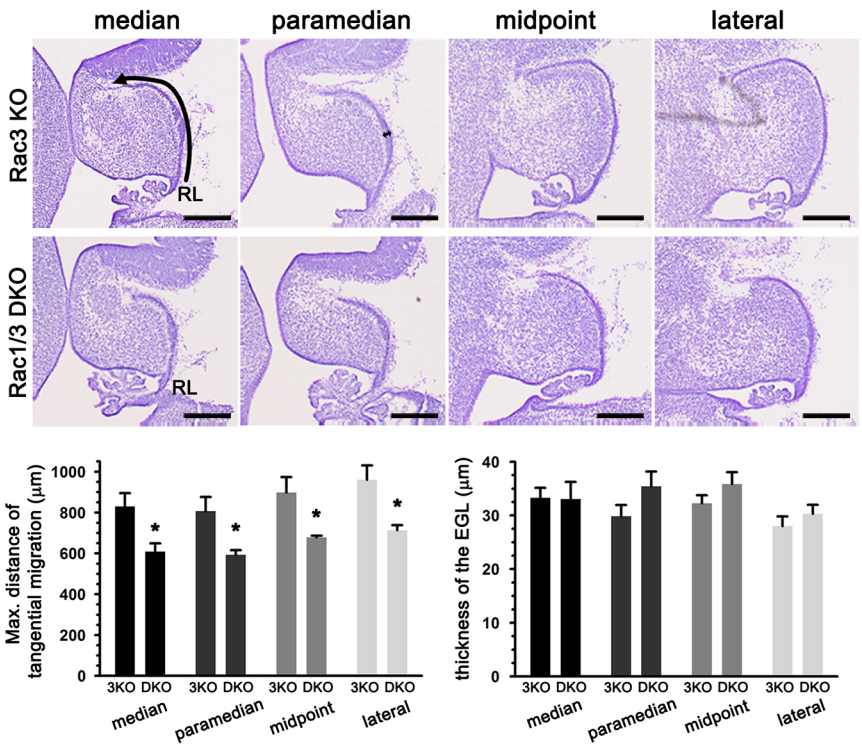

Fig. 5. Impaired tangential migration in the *Atoh1-Cre;Rac1$^{flox/flox}$;Rac3$^{-/-}$* cerebellum. Four sagittal sections of the cerebellum were obtained from *Rac1$^{flox/flox}$;Rac3$^{-/-}$* (*Rac3* KO) and *Atoh1-Cre;Rac1$^{flox/flox}$;Rac3$^{-/-}$* (*Rac1*/*Rac3* DKO) mice at E16.5. The longest distance over which CGN progenitors tangentially migrate from the RL (indicated by the arrow) and the maximum thicknesses of the EGL (bi-directional arrows) were quantified (n=6 for each section from three mice, *P<0.05 using Bonferroni's post-hoc test following two-way ANOVA). Scale bars: 250 μm.

P5. All CGNs in the EGL were Pax6 positive (Fig. 7A), whereas CGNs in the lower one-third to one half of the EGL were strongly p27^{Kip1} positive (Fig. 7C). CGNs in the very lowest region (rows 1-3) of the EGL were strongly NeuN positive (Fig. 7D). No significant difference in cerebellar immunostaining for any marker was observed between *Atoh1-Cre;Rac1$^{flox/flox}$;Rac3$^{-/-}$* and *Rac1$^{flox/flox}$;Rac3$^{-/-}$* mice (Fig. 7A-D). The ratio of cell numbers (p27^{Kip1}/DAPI and NeuN/DAPI) in the EGL (statistically analyzed in the anterior and posterior lobe of cerebellum) did not significantly differ between *Rac1$^{flox/flox}$;Rac3$^{-/-}$* and *Atoh1-Cre;Rac1$^{flox/flox}$;Rac3$^{-/-}$* mice (Fig. 7B,C). All lobules (I-X) were observed in the *Atoh1-Cre;Rac1$^{flox/flox}$;Rac3$^{-/-}$* cerebellum (Fig. 7B).

These results suggest that *Atoh1-Cre;Rac1$^{flox/flox}$;Rac3$^{-/-}$* CGNs undergo apoptosis following differentiation, which appears normal until expression of NeuN occurs.

Requirement of Rac for neuritogenesis and migration of CGNs

To examine neuritogenesis in Rac-deleted CGNs, we used primary cultures of CGNs. Using βIII-tubulin immunostaining, we observed that *Atoh1-Cre;Rac1$^{flox/flox}$* CGNs exhibited moderately impaired neuritogenesis compared with *Rac1$^{flox/flox}$* and *Rac1$^{flox/flox}$;Rac3$^{-/-}$* CGNs, and that this impairment was exacerbated in *Atoh1-Cre;Rac1$^{flox/flox}$;Rac3$^{-/-}$* CGNs (Fig. 8A).

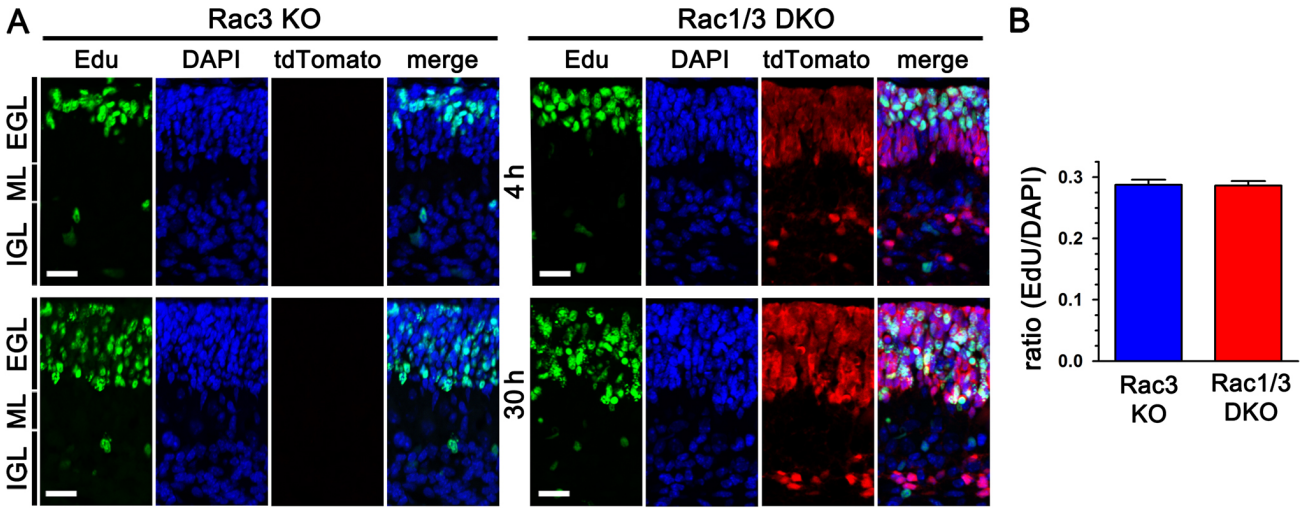

Fig. 6. Normal proliferation of CGNs in the *Atoh1-Cre;Rac1$^{flox/flox}$;Rac3$^{-/-}$* cerebellum. (A) EdU was injected into *Rac1$^{flox/flox}$;Rac3$^{-/-}$* (*Rac3* KO) and *Atoh1-Cre;Rac1$^{flox/flox}$;Rac3$^{-/-}$* (*Rac1*/*Rac3* DKO) mice at P4, and samples were fixed at 4 h and 30 h after injection. Sagittal sections of the anterior cerebellar lobe of *Rac3*-KO and *Rac1*/*Rac3*-DKO mice were obtained. Scale bars: 50 μm. (B) EdU labeling index (ratio of Edu-Alexa488-positive cells/DAPI-positive cells) at the EGL 4 h after EdU injection (n=12 from two mice). EGL, external granule layer; ML, molecular layer; IGL, internal granule layer.

Development (2017) 144, 1863-1875 doi:10.1242/dev.147900

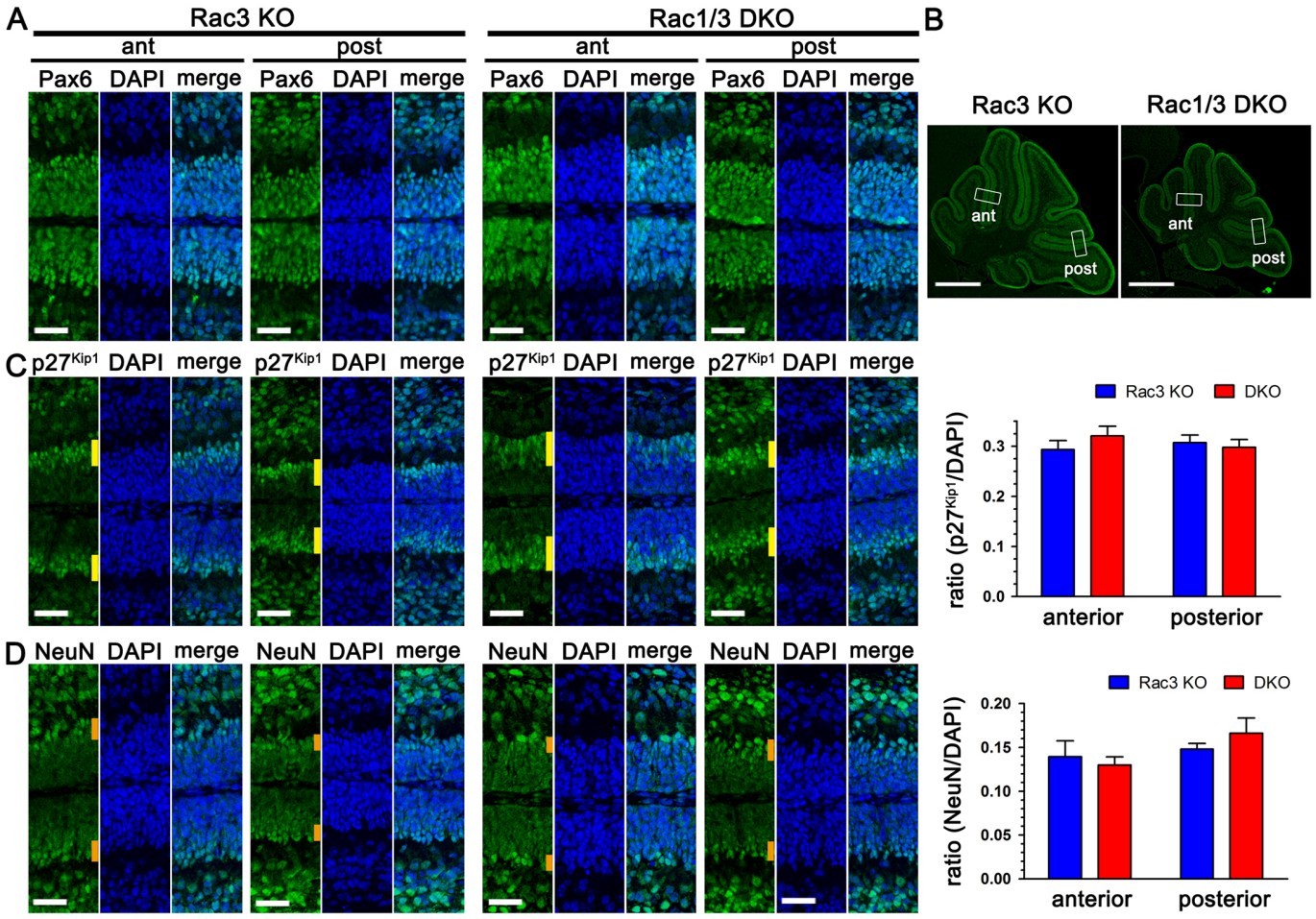

Fig. 7. Normal development of CGNs in the *Atoh1-Cre;Rac1$^{flox/flox}$;Rac3$^{-/-}$* cerebellum. (A-D) *Rac1$^{flox/flox}$;Rac3$^{-/-}$* (*Rac3* KO) and *Atoh1-Cre;Rac1$^{flox/flox}$;Rac3$^{-/-}$* (*Rac1*/*Rac3* DKO) mice were fixed at P5. Sagittal sections of *Rac3*-KO and *Rac1*/*Rac3*-DKO cerebella were stained with a Pax6 antibody (A,B), a p27^{Kip1} antibody (C) and a NeuN antibody (D). (A,C,D) Magnified images of the anterior (ant) and posterior (post) lobes indicated by rectangles in B are shown. (A) All CGNs in the EGL are Pax6 positive. (B) Lobules I-X are observed in the cerebellum of both *Rac3-KO* and *Rac1*/*Rac3*-KO mice. (C) CGNs in the lower one-third to one-half of the EGL (indicated by yellow lines) are strongly positive for p27^{Kip1} (*n*=12 for each region from two mice). (D) CGNs in the lowest region (rows 1-3; indicated by orange lines) of the EGL are strongly positive for NeuN (*n*=12 for each region from two mice). Scale bars: 25 µm in A,C,D; 500 µm in B. The graphs show the ratio of cell numbers in the EGL (C, p27^{Kip1}/DAPI and D, NeuN/DAPI).

We then used cerebellar microexplant cultures to further investigate the involvement of Rac in neuritogenesis and migration. Previous research has indicated that, after their final mitosis, CGNs remain in the EGL for 20-48 h. During this period, CGNs change their morphology from round to unipolar to bipolar to tripolar. In the bipolar phase, CGNs reach the deep layer of the EGL. CGNs then inwardly extend a single vertical process and initiate radial migration to form the IGL (Komuro et al., 2001). The horizontal and vertical processes of CGNs are reported to differentiate into the parallel fiber axons and dendrites, respectively (Kawaji et al., 2004). Parallel neurites projecting from the microexplant and neurites perpendicular to the parallel neurites have been reported to mimic the horizontal axons and vertical dendrites of CGNs *in vivo*, respectively. Biphasic migration, which includes early migration along the parallel neurites and later migration along the perpendicular neurites, observed in the microexplant culture have been used as models of tangential and radial migration *in vivo*, respectively (Kawaji et al., 2004). The parallel neurite length stained by βIII-tubulin projected from the microexplant (Fig. 8B) and tangential migration, defined as the migration distance along the parallel neurite from the microexplant (Fig. 8B and Fig. S3A), were significantly shorter in *Atoh1-Cre;Rac1$^{flox/flox}$;Rac3$^{-/-}$* microexplants than in *Rac1$^{flox/flox}$;Rac3$^{-/-}$* microexplants. Furthermore, although *Rac1$^{flox/flox}$;Rac3$^{-/-}$* microexplants exhibited regularly aligned parallel neurite bundles in combination with Map2-positive perpendicular neurites, *Atoh1-Cre;Rac1$^{flox/flox}$;Rac3$^{-/-}$* microexplants exhibited impaired alignment of βIII-tubulin-positive neurites with few Map2-positive neurites (Fig. 8C), suggesting severely impaired dendritic development and radial migration in *Atoh1-Cre;Rac1$^{flox/flox}$;Rac3$^{-/-}$* CGNs.

Disrupted vertical neurites in *Rac1*/*Rac3*-DKO CGNs *in vivo*

Next, we examined the vertical neurites projecting from CGNs for radial migration *in vivo* using *Atoh1-Cre;Rac1$^{flox/flox}$;Rac3$^{-/-}$;tdTomato* mice, in which *Rac1*/*Rac3*-DKO CGNs were labeled by tdTomato fluorescence.

Because tdTomato fluorescence in neurites of CGNs was not strong enough for detailed evaluation, and because Map2 immunostaining exhibits a strong non-specific background, tdTomato fluorescence from vertical neurites was enhanced by immunostaining using an RFP polyclonal antibody. Although

Development (2017) 144, 1863-1875 doi:10.1242/dev.147900

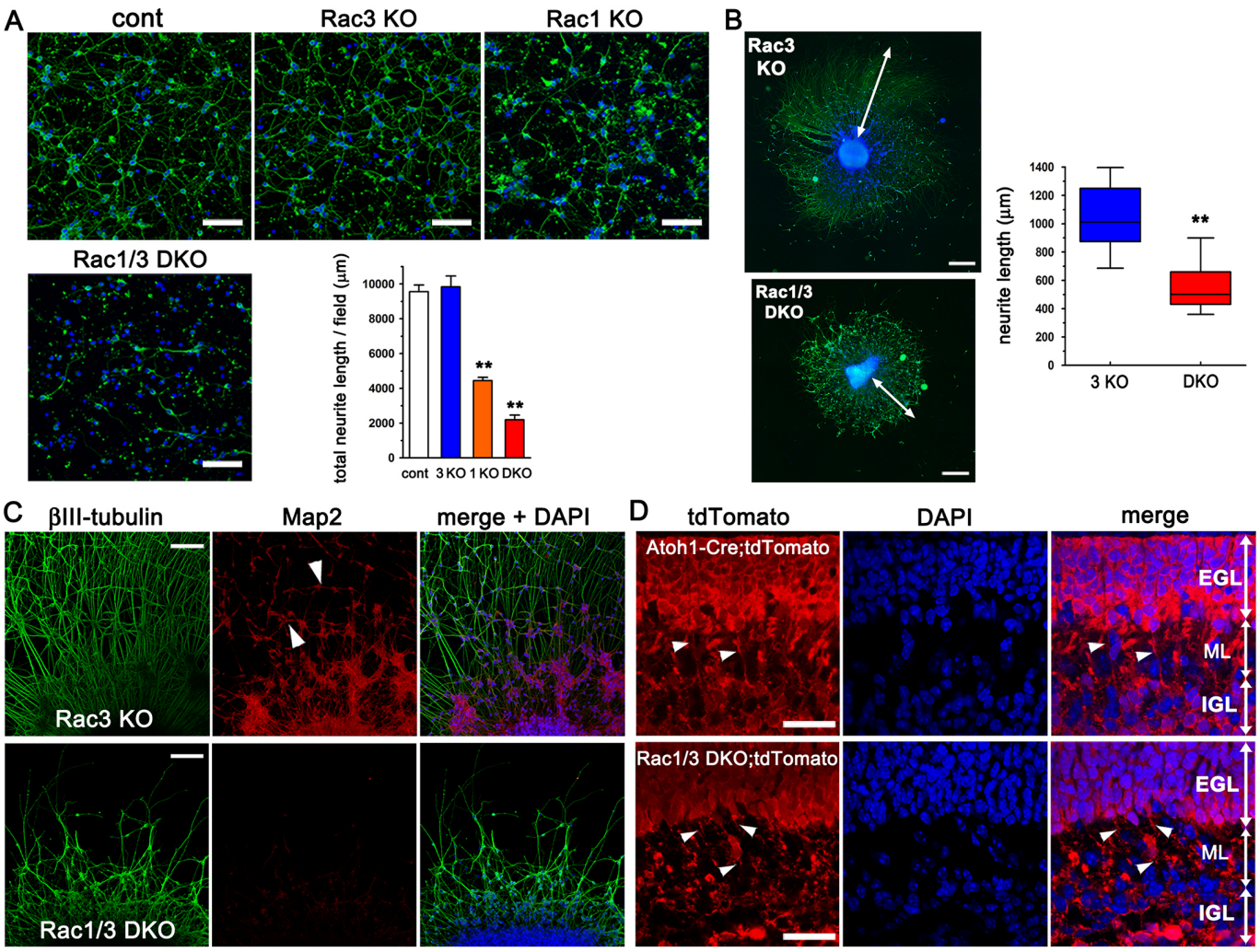

Fig. 8. Impaired dendritogenesis in *Atoh1-Cre;Rac1$^{flox/flox}$;Rac3$^{-/-}$* cerebellar microexplant and impaired development of vertical neurites of CGNs in the *Atoh1-Cre;Rac1$^{flox/flox}$;Rac3$^{-/-}$* cerebellum. (A) After 7 days in culture, primary CGNs from four mouse lines were fixed and stained using a βIII-tubulin antibody and DAPI. The total neurite length was quantified (n=5, $^{**}P$<0.01 using Bonferroni's post-hoc test following one-way ANOVA). Scale bars: 50 µm. (B,C) After 3 days in culture, cerebellar microexplants from *Rac1$^{flox/flox}$;Rac3$^{-/-}$* (*Rac3* KO) and *Atoh1-Cre;Rac1$^{flox/flox}$;Rac3$^{-/-}$* (*Rac1*/*Rac3* DKO) mice were fixed and stained using a βIII-tubulin antibody and DAPI (B), or using βIII-tubulin and Map2 antibodies and DAPI (C). (B) The longest neurite lengths indicated by bi-directional arrows (n=17 microexplants from six mice) were quantified ($^{**}P$<0.01 using the Kolmogorov–Smirnov test). Scale bars: 300 µm. (C) Note the low amount of Map2 immunoreactivity in the image of the *Rac1*/*Rac3*-DKO microexplant, which was obtained using the same image acquisition parameters used for imaging of the *Rac3*-KO microexplant (arrowheads). Scale bars: 100 µm. n=5. (D) Sagittal sections of *Atoh1-Cre;tdTomato* (control) and *Atoh1-Cre;Rac1$^{flox/flox}$;Rac3$^{-/-}$;tdTomato* (*Rac1*/*Rac3* DKO;tdTomato) mice at P8 were stained using an RFP antibody with DAPI. Arrowheads indicate tdTomato-positive vertical neurites inwardly projecting from radially migrating CGNs in the anterior lobe. The tdTomato-positive vertical neurites are difficult to observe in *Rac1*/*Rac3*-DKO mice. EGL, external granule layer; ML, molecular layer; IGL, internal granule layer. Scale bars: 25 µm. n=3.

vertical neurites became visible, horizontal neurites were impossible to evaluate due to the strong tdTomato fluorescence from crowded somata of CGNs in the EGL. Vertical inward neurites projecting from radially migrating CGNs were observed in the *Atoh1-Cre;tdTomato* cerebellum at P8 (Fig. 8D). In sharp contrast, they were short and poorly visualized in the anterior medial cerebellum of *Atoh1-Cre;Rac1$^{flox/flox}$;Rac3$^{-/-}$;tdTomato* mice (Fig. 8D). However, vertical neurites were visible in the posterior medial *Atoh1-Cre;Rac1$^{flox/flox}$;Rac3$^{-/-}$;tdTomato* cerebellum (Fig. S3B).

Rac enhances the transcription of Mid1

To verify the underlying mechanism of impaired development of the anterior medial cerebellum in *Atoh1-Cre;Rac1$^{flox/flox}$;Rac3$^{-/-}$* mice, we applied DNA microarray analyses to the medial cerebellum at P6, which is just prior to the robust radial migration of CGNs (Hatten et al., 1997) and the emergence of the *Atoh1-Cre;Rac1$^{flox/flox}$;Rac3$^{-/-}$* phenotypes. Among the genes upregulated or downregulated by more than threefold in the *Atoh1-Cre;Rac1$^{flox/flox}$;Rac3$^{-/-}$* cerebellum relative to the *Rac1$^{flox/flox}$;Rac3$^{-/-}$* cerebellum, we focused on those encoding cytoskeleton-associated proteins. We revealed that *Mid1*, which is responsible for abnormalities in midline structures observed in OS, was decreased in the *Atoh1-Cre;Rac1$^{flox/flox}$;Rac3$^{-/-}$* cerebellum compared with control (0.297-fold when normalized using the 75th percentile, 0.289-fold when normalized to *Actg1* and 0.297-fold when normalized to *Tuba1a*). The effect of *Rac* KO on *Mid1* expression detected by DNA microarray analyses was confirmed in the dissected cerebellar cortex, which mainly consists of the EGL, using quantitative PCR (qPCR) (Fig. 9A). Furthermore, we

Development (2017) 144, 1863-1875 doi:10.1242/dev.147900

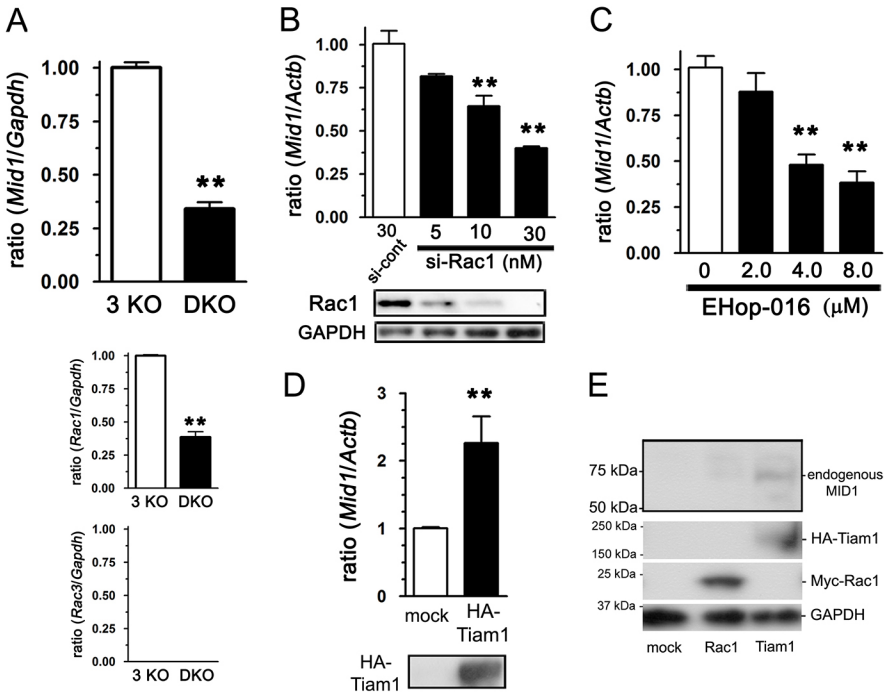

Fig. 9. Mid1 expression is transcriptionally regulated by Rac. (A) Total RNA was isolated from the dissected cerebellar cortex of *Rac1*$^{flox/flox}$;*Rac3*$^{-/-}$ (*Rac3* KO) and *Atoh1-Cre;Rac1*$^{flox/flox}$;*Rac3*$^{-/-}$ (*Rac1*/*Rac3* DKO) mice at P6. Decreases in levels of *Mid1*, *Rac1* and *Rac3* mRNA were quantified using qPCR (n=3, **P<0.01). (B) Forty-eight hours after electroporation of si-Rac1 in RN46A cells, decreases in levels of *Mid1* mRNA were quantified using qPCR (n=3, **P<0.01). Knockdown of *Rac1* was confirmed via immunoblotting. (C) Twenty-four hours after treatment of RN46A cells with the indicated concentration of a Rac-specific inhibitor, EHop-016. Decreases in levels of *Mid1* mRNA were quantified using qPCR (n=6, **P<0.01). (D) Forty-eight hours after mock electroporation or electroporation of HA-Tiam1 into RN46A cells, increases in levels of *Mid1* mRNA following HA-Tiam1 transfection were quantified using qPCR (n=6, **P<0.01). (E) Mock, Myc-Rac1 and HA-Tima1 plasmids were transfected into HEK293 cells. Forty-eight hours after transfection, lysates were immunoblotted using Mid1, Myc and HA antibodies. Endogenous *Mid1* expression increased slightly following Myc-Rac1 transfection and slightly more following HA-Tiam1 transfection. n=3. Student's t-test and Bonferroni's post-hoc test following one-way ANOVA were applied to A and D, and B and C, respectively.

confirmed specific localization of *Mid1* mRNA in the EGL as well as decreased *Mid1* mRNA in both the EGL of the anterior and posterior lobe of the cerebellum in *Atoh1-Cre;Rac1*$^{flox/flox}$;*Rac3*$^{-/-}$ mice using *in situ* hybridization (Fig. S4).

Because the thickness of the medial IGL in the *Atoh1-Cre;Rac1*$^{flox/flox}$ cerebellum was 25-30% of that in the control (*Rac3*-KO) cerebellum (Fig. 2B), we expected that the transcriptional regulation of *Mid1* by Rac could be determined by the knockdown (KD) experiment of Rac1 using a validated Rac1-siRNA (Ueyama et al., 2006). A mild decrease in *Mid1* mRNA in response to Rac1 KD was observed in rat-derived RN46A neuronal cells using qPCR (Fig. 9B). Transcriptional regulation of *Mid1* by Rac was further confirmed by the following results in RN46A cells: decreased *Mid1* mRNA levels following treatment with a novel Rac-specific inhibitor (EHop-016; Fig. 9C); and increased *Mid1* mRNA levels following expression of a Rac-specific guanine nucleotide-exchange factor (GEF) (Tiam1; Fig. 9D). Increases in Mid1 protein levels following expression of Tiam1 were confirmed in human-derived HEK293 cells (Fig. 9E).

Rac-Mid1-mTORC1 is a novel signal axis involved in the neurite outgrowth of CGNs

Most mammals have a basic pattern of 10 major lobules (I-X) in the cerebellar vermis. We demonstrated that *Atoh1-Cre;Rac1*$^{flox/flox}$;*Rac3*$^{-/-}$ mice exhibited agenesis of the IGL, predominantly in the anterior medial cerebellum. Similarities in abnormal alterations observed in the anterior medial cerebellum of *Mid1*-KO mice (I-III) (Lancioni et al., 2010) and our *Atoh1-Cre;Rac1*$^{flox/flox}$;*Rac3*$^{-/-}$ mice (I-VII) prompted us to further examine the function and signaling of Mid1 in CGNs. Normal development of the posterior medial cerebellum in both *Mid1*-KO mice and *Atoh1-Cre;Rac1*$^{flox/flox}$;*Rac3*$^{-/-}$ mice may be explained by the lateral-to-medial movement of CGNs that specifically occurs in the posterior lobe during cerebellar development (Chédotal, 2010; Sgaier et al., 2005).

A recent study demonstrated that inhibition/depletion of Mid1 results in the downregulation of mTORC1 signaling (Liu et al., 2011). This report prompted us to examine a new signaling pathway: Rac1-Mid1-mTORC1. In rat-derived PC12 neuronal cells with *Rac1* KD, the protein levels of Ppp2ca, a well-established target of Mid1, were increased relative to control (Fig. 10A). In addition, levels of S6 ribosomal protein and 4E-BP1 phosphorylation, which are well-known downstream targets of mTORC1, were decreased (Fig. 10A). The decreased levels of *Mid1* were confirmed using qPCR (Fig. 10A). Decreased levels of Mid1 and mTORC1 signaling (represented by the decreased phosphorylation of 4E-BP1) following *Rac* deletion were observed in both the medial and lateral cerebellum of *Atoh1-Cre;Rac1*$^{flox/flox}$;*Rac3*$^{-/-}$ mice, using the dissected cerebellar cortex, which mainly consists of the EGL (Fig. 10B). Taken together, these results indicate that *Rac* is involved in the regulation of the Mid1-mTORC1 signaling axis.

Finally, we examined the effects of *Mid1* KD on neuritogenesis, mTORC1 signaling and migration using mouse primary CGNs and microexplants. Two effective siRNAs for *Mid1*, *siMid1-832* and *siMid1-1107* (Fig. 10C) revealed a mild reduction of neuritogenesis (Fig. 10C). The decreased levels of *Mid1* were confirmed using qPCR (Fig. 10C). A similar *Mid1*-KD effect on neuritogenesis was also observed in the experiment using rat primary CGNs and rat-specific siRNA for *Mid1* (Fig. 10D). The increased levels of Ppp2ca and the reduced mTORC1 signaling (represented by decreases in the phosphorylation of S6 ribosomal protein) were also confirmed in *Mid1*-KD (*siMid1-832*) primary CGNs (Fig. 10E). Furthermore, decreased cell migration was observed in *Mid1*-KD CGNs of microexplant cultures (Fig. S5).

DISCUSSION

In the present study, we revealed that both *Rac1* and *Rac3* mRNAs are expressed at the highest levels in CGNs during cerebellar development. Notably, although *Rac1* mRNA was still expressed in CGNs at P21, *Rac3* mRNA expression disappeared following cerebellar development. Furthermore, the phenotypes of *Rac1*-KO mice were exacerbated and became tangible by the additional KO of

Development (2017) 144, 1863-1875 doi:10.1242/dev.147900

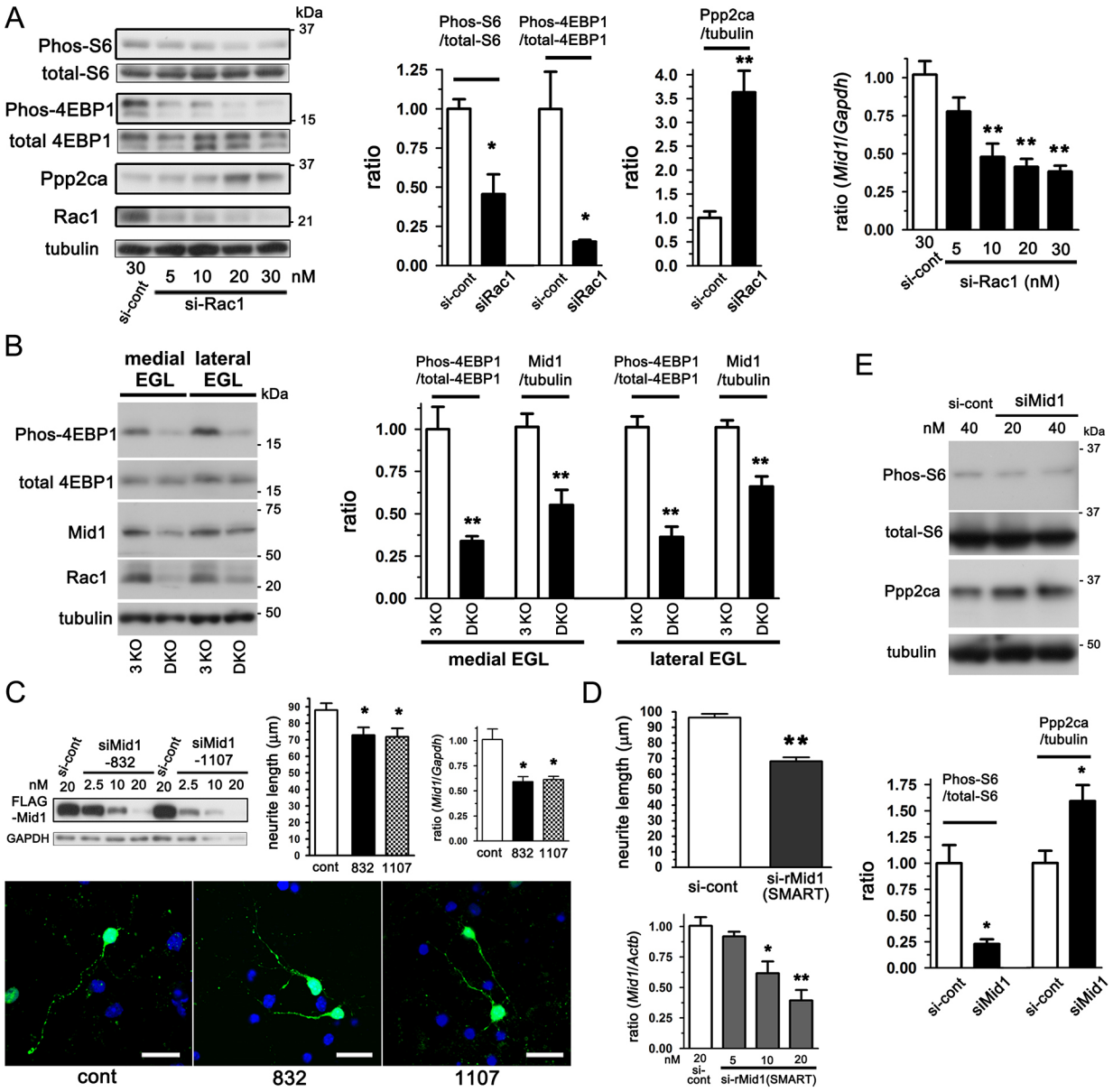

Fig. 10. The Rac1-Mid1-mTORC1 axis is a novel signaling pathway involved in the neuritogenesis of CGNs. (A) Forty-eight hours after electroporation of the indicated concentration of si-Rac1 in PC12 cells, the levels of Rac1, Ppp2ca, phosphorylated S6 ribosomal protein (Phos-S6) and phosphorylated 4E-BP1 (Phos-4EBP1) were examined via immunoblotting. Decreases in Phos-S6 and Phos-4EBP1, and increases in Ppp2ca levels at 30 nM si-Rac1 were quantified (n=3, *P<0.05 and **P<0.01; Student's t-test). Decreases in the levels of *Mid1* mRNA were confirmed using qPCR (n=6, **P<0.01). (B) The levels of Mid1 and Phos-4EBP1 protein were examined in the dissected medial and lateral cerebellar EGLs of $Rac1^{flox/flox}$;$Rac3^{-/-}$ (*Rac3*-KO) and *Atoh1-Cre*;$Rac1^{flox/flox}$ (*Rac1*/*Rac3* DKO) mice at P4 via immunoblotting. Decreases in Phos-4EBP1 and Mid1 levels in the medial and lateral EGLs were quantified (n=3, **P<0.01; Student's t-test). (C) The efficacy of two *Mid1* siRNAs (832 and 1107) was confirmed using HEK293 cells with co-transfection of FLAG-tagged mMid1. Forty-eight hours after electroporation of siRNAs (20 nM) in combination with a pEGFP plasmid, mouse primary CGNs were fixed. The longest neurite length of EGFP-positive CGNs was quantified (n=60 from three independent experiments, *P<0.05). The longest neurites were shortened by two si-Mid1s, shown as representative images. Efficient knockdown of *Mid1* by two *siMid1s* in primary CGNs was confirmed using qPCR (n=3, *P<0.05). Scale bars: 25 μm. (D) siRNA (20 nM control or 20 nM siRNA for rat *Mid1* [SMARTpool])+pEGFP plasmid was electroporated into primary rat CGNs. The longest neurite length of EGFP-positive CGNs was quantified (n≥60, *P<0.01; Student's t-test). The longest neurites were shortened by si-rMid1. The efficacy of rat *Mid1* siRNA was confirmed via qPCR using PC12 cells (n=3, *P<0.05 and **P<0.01). (E) Forty-eight hours after electroporation of the indicated concentration of siRNAs into mouse primary CGNs, levels of Ppp2ca and Phos-S6 were examined via immunoblotting. Decreases in Phos-S6 and increases in Ppp2ca levels at 40 nM siMid1-832 were quantified (n=3, *P<0.05; Student's t-test). Bonferroni's post-hoc test following one-way ANOVA was applied to A-E unless undefined.

Rac3. These results suggest that both Rac1 and Rac3 function in CGNs during cerebellar development, and that Rac3 is particularly important for CGNs in this period.

Although we demonstrated that both axonogenesis and dendritogenesis, and both tangential and radial migration were impaired in *Rac1*/*Rac3*-DKO mice, dendritogenesis and radial migration were more severely impaired both *in vitro* (cerebellar microexplant) and *in vivo* (cerebellum). Our findings are in accordance with those of previous reports that have revealed: (1) decreased levels of Map2 and impaired dendrite branching in primary CGNs from *Vav3*, a GEF for Rac, KO mice (Quevedo et al., 2010); (2) impaired dendritogenesis but not axonogenesis in *Rac1*-KD primary

Development (2017) 144, 1863-1875 doi:10.1242/dev.147900

hippocampal neurons from *Rac3*-KO mice (Gualdoni et al., 2007); (3) Rac activation by laminin (Gu et al., 2001); and (4) radial migration observed only on laminin-coated dishes in cerebellar microexplant cultures (Kawaji et al., 2004; Nagata and Nakatsuji, 1990).

CGN progenitors migrate tangentially from the RL to form the EGL during the initial stage of cerebellar development (until E16.5) (Sgaier et al., 2005). Rac1-dependency in the tangential migration of olfactory and cortical interneurons has been reported (Chen et al., 2007). In the present study, we demonstrated impaired tangential migration during the formation of the most anterior region of the cerebellar primordium, which requires the longest path of migration, in *Rac1/Rac3*-DKO mice at E16.5. Because lobules I-X and their EGL were formed at P5, the impaired tangential migration may be related only to the smaller size of the *Rac1/Rac3*-DKO cerebellum. Impaired differentiation and apoptosis have been reported in Rac1-KO telencephalon-derived neurons (Chen et al., 2009). In addition, selective inhibition of Rac has been reported to induce apoptosis in CGNs (Stankiewicz et al., 2015). *Rac1/Rac3*-DKO CGNs exhibited: (1) a normal pattern of differentiation until the expression of NeuN, a marker for postmitotic CGNs, was seen in the deepest layer of the EGL at P5; (2) few Map2-positive neurites in cerebellar microexplants and disrupted development of vertical dendrites at P8; and (3) robust apoptosis at the deep layer of the EGL, a premigratory zone for preparing the subsequent radial migration (Yamasaki et al., 2001), at P8. Such results suggest that agenesis of the IGL is due to disruption of the radial migration in CGNs, which is caused by impaired final differentiation of CGNs with dendritogenesis. However, the precise cause of apoptosis in the premigratory zone of the EGL remains unknown.

In the present study, we revealed that Mid1 is a novel and transcriptionally regulated downstream target of Rac. The dynamic phosphorylation/dephosphorylation cycles regulated by Pp2a, a well-established downstream target of Mid1, play important roles in neuronal functions, including migration, neurite initiation and protein synthesis (Ayala et al., 2007; Basu, 2011; Laplante and Sabatini, 2012). Previous studies have reported that 4E-BP1, which is a phosphorylation target of mTORC1 for the promotion of protein synthesis (Nanahoshi et al., 1998), and Map2, which is a well-known dendrite marker involved in neurite outgrowth (Sanchez et al., 2000), are Pp2a targets. Indeed, we observed impairments in mTORC1 signaling and Map2 expression (dendritogenesis) via *Rac* KD and KO. The protein mTOR assembles into two complexes, mTORC1 and mTORC2, which can be distinguished by their associated proteins, raptor (Rptor) and rictor, respectively (Laplante and Sabatini, 2012). A recent study showed that neuron-specific inactivation of mTORC2 following *Rictor* KO resulted in a small brain, including a small cerebellum, although the development of the medial IGL was normal (Thomanetz et al., 2013). Meanwhile, another study revealed that neuron-specific inactivation of mTORC1 following *Rptor* KO resulted in microcephaly and lethality within a few hours of birth, prior to the completion of cerebellar development (Cloetta et al., 2013). These reports exclude the involvement of mTORC2, but not of mTORC1, signaling in CGNs of the medial cerebellum. *Rptor*-KO mice also exhibit reduced Map2 staining and reduced dendritic complexity in the cerebral cortex (Cloetta et al., 2013). Additionally, Mid1 has been reported to regulate the interaction between mTOR and raptor (Liu et al., 2011), and to regulate microtubule-associated mRNA transport and protein translation (Aranda-Orgillés et al., 2008). Activation of mTORC1 by brain-derived neurotrophic factor (BDNF), which induces Rac activation (Yoshizawa et al., 2005), has been reported to be involved in local protein synthesis in neuronal dendrites (Takei et al., 2004). Impaired protein synthesis in dendrites through impaired Rac-Mid1-mTORC1 signaling may be one of the causes of impaired dendritogenesis and apoptosis of *Rac1/Rac3*-DKO CGNs in the deep layer, a premigratory zone, of the EGL. However, rescue experiments using GFP-Mid1 into *Rac1/Rac3*-DKO primary CGNs showed no recovery of impaired neuritogenesis. Although relatively weak involvement of Rac1-mediated transcriptional regulation of Mid1 cannot be completely excluded, these results suggest the following possibilities: (1) in spite of the involvement of Mid1 in neuritogenesis, migration and mTORC1 signaling, Rac is more crucially and broadly involved in these functions than Mid1; and (2) Rac, Mid1 and mTORC1 synergistically act to carry out these functions. Indeed, the extent of cerebellar agenesis in *Rac1/Rac3*-DKO mice (I-VII) was greater than that of agenesis/hypoplasia reported in the *Mid1*-KO cerebellum (I-III) (Lancioni et al., 2010). Moreover, we identified the possibility that Rac1/Mid1/mTOR functions as a complex (Fig. S6), in accordance with the findings of previous reports: interactions of Mid1 with mTORC1 (Liu et al., 2011) and Rac1 with mTOR (Saci et al., 2011).

The most frequent CNS phenotype of OS involves agenesis/hypoplasia of the cerebellar vermis, followed by agenesis/hypoplasia of the corpus callosum (Fontanella et al., 2008; Pinson et al., 2004), suggesting that the activity of Mid1 in neurons may be modulated by other factors. Indeed, researchers have revealed agenesis of the vermis (Lancioni et al., 2010) and mild abnormalities in the corpus callosum (Lu et al., 2013) in *Mid1*-KO mice. In the latter study, elongated axons were observed in *Mid1*-KD/*Mid1*-KO cortical neurons (Lu et al., 2013). The cause of the discrepancy between the present study, which revealed impaired neuritogenesis following *Mid1* KD, and the latter study remains unknown, although it may be related to differences in the specificity of cortical neurons and CGNs. Alternatively, the activation states of Rac and redundancy of Mid2 (Short et al., 2002) may vary according to the neuronal type/brain region, as well as developmental stage, inducing variable expressivity of OS phenotypes. In any case, phenotypes of *Rac1/Rac3*-DKO and OS are restricted to the midline. However, we observed that Mid1 and Rac are expressed not only in the medial structures but also the lateral structures/regions (Fig. 10B). Moreover, Mid1 expression and mTORC1 signaling in the *Rac1/Rac3*-DKO cerebellum was reduced in both the medial and lateral EGL. Such evidence strongly suggests that a specific molecule(s)/signaling(s) exists to regulate the function of Mid1 only around the medial structures of the body. In the present study, we were unable to identify additional factor(s) responsible for the restriction of lesions in OS. However, our findings indicate that Rac1 regulates levels of Mid1 expression and functions synergistically in a complex with Mid1 and mTORC1. A previous study using Nestin-Cre-driven *Rac1*-KO mice focused on impaired axon formation and neuronal migration in CGNs; however, the authors reported more modest medial cerebellar agenesis (II-V) than that observed in our *Rac1/Rac3*-DKO mice (I-VII), without referring to any mechanism (Tahirovic et al., 2010). The novel Rac-Mid1-mTORC1 signaling pathway proposed for midline structures in the present study may be further supported by the findings that telencephalon-specific *Rac1*-KO mice exhibit agenesis of the corpus callosum (Chen et al., 2007; Kassai et al., 2008).

MATERIALS AND METHODS

Animals

Atoh1-Cre transgenic (TG) mice (Matei et al., 2005) and *Rac1*$^{flox/flox}$ mice (Kassai et al., 2008) were backcrossed to generate *Atoh1-Cre;Rac1*$^{flox/flox}$ mice. *Atoh1-Cre;Rac1*$^{flox/flox}$ mice and *Rac3*$^{-/-}$ mice (Corbetta et al., 2005) were backcrossed for more than five generations to obtain experimental animals (*Rac*$^{flox/flox}$*;Rac3*$^{-/-}$, *Atoh1-Cre;Rac*$^{flox/+}$*;Rac3*$^{-/-}$, *Atoh1-Cre;*

Development (2017) 144, 1863-1875 doi:10.1242/dev.147900

Rac1$^{flox/flox}$;*Rac3*$^{-/+}$ and *Atoh1-Cre;Rac1*$^{flox/flox}$;*Rac3*$^{-/-}$). *CAG-STOP*^{flox}-*dtTomato* (Ai9) TG reporter mice were purchased from the Jackson Laboratory and backcrossed with *Atoh1-Cre* mice and *Atoh1-Cre;Rac1*$^{flox/flox}$;*Rac3*$^{-/-}$ mice. See the supplementary Materials and Methods for further details of genotyping.

Cells, chemicals, plasmids and RNA interference

RN46A (Sakai et al., 2003), PC12 (Sakai et al., 2003) and HEK293 (ATCC) cells were used in the present study (for details on cell maintenance, see the supplementary Materials and Methods). EHop-016, which inhibits Rac GEF interaction and has 100-fold higher specificity than the established Rac inhibitor NSC23766 (Montalvo-Ortiz et al., 2012), was obtained from Millipore. The details of plasmids and RNA interference are described in the supplementary Materials and Methods.

In situ hybridization

In situ hybridization was performed as previously described (Ueyama et al., 2014) using P6 and P21 wild-type mice and a pair of *Rac1*$^{flox/flox}$;*Rac3*$^{-/-}$ and *Atoh1-Cre;Rac1*$^{flox/flox}$;*Rac3*$^{-/-}$ mice at P5. See the supplementary Materials and Methods for details of DNA probes.

qPCR and RT-PCR

Total RNA was extracted using an RNeasy Mini kit (Qiagen). Reverse transcription was performed on 1-5 µg of total RNA using SuperScript III reverse transcriptase (Invitrogen) and random primers. qPCR was performed using gene-specific primers (*Mid1*, *Rac1*, *Rac3*, *Actb* and *Gapdh*) as previously described (Ueyama et al., 2016). Details of primers used for qPCR and RT-PCR can be found in the supplementary Materials and Methods.

Immunoblotting and antibodies

Immunoblotting was performed as previously described (Ueyama et al., 2016). For details of antibodies used in immunoblotting and histochemistry, see the supplementary Materials and Methods.

Section preparation and histochemistry

Sections were prepared as previously described (Ishii et al., 2017). Nissl staining was performed using Cresyl Violet solution (Muto Pure Chemicals). P8 cerebellar sections were used for detecting apoptosis via active caspase 3 immunostaining, followed by diaminobenzidine staining using a Vectastain ABC kit (Vector Laboratories) and Hematoxylin counterstaining. P5 sections obtained from *Rac1*$^{flox/flox}$;*Rac3*$^{-/-}$;*tdTomato* and *Atoh1-Cre;Rac1*$^{flox/flox}$;*Rac3*$^{-/-}$;*tdTomato* cerebellum were immunostained for Pax6, p27^{Kip1} and NeuN to evaluate the differentiation of CGNs. P8 sections obtained from *Atoh1-Cre;tdTomato* and *Atoh1-Cre;Rac1*$^{flox/flox}$;*Rac3*$^{-/-}$;*tdTomato* cerebellum were used for immunofluorescence imaging of vertical neurites projecting from radially migrating GCNs. Coronal cerebellar sections obtained from 12-week-old *Rac1*$^{flox/flox}$;*Rac3*$^{-/-}$;*tdTomato* and *Atoh1-Cre;Rac1*$^{flox/flox}$;*Rac3*$^{-/-}$;*tdTomato* mice were immunostained for calbindin. Samples were imaged using a light microscope with a DP26 camera (Olympus) or a LSM700 confocal laser microscope (Carl Zeiss).

EdU pulse labeling

P4 mice (*Atoh1-Cre;Rac1*$^{flox/flox}$;*Rac3*$^{-/-}$;*tdTomato* and *Rac1*$^{flox/flox}$;*Rac3*$^{-/-}$;*tdTomato*) were intraperitoneally injected with 15 mg/kg 5-ethynyl-2′-deoxyuridine (EdU) dissolved in PBS. For the analysis of proliferation of CGNs in the EGL, cerebella were fixed 4 h after injection. For the analysis of radial migration of CGNs, cerebella were fixed 30 h after injection. In sagittal sections (8 µm), EdU detection was performed using a Click-iT EdU Alexa Fluor 488 Imaging kit (Invitrogen) and a confocal laser microscope. The EdU labeling index was defined as the ratio of EdU-Alexa488-labeled cells/DAPI-labeled cells.

Preparation of primary CGNs and cerebellar microexplants

Primary CGN cultures and cerebellar microexplant cultures (Nagata and Nakatsuji, 1990) were generated according to a previously described protocol.

For primary CGN cultures, the P8 cerebellum was dissected and dissociated with 0.25% trypsin. Washed and centrifuged cells mixed in DMEM supplemented with B27 (Invitrogen) were plated on poly-D-lysine (PDL)-coated Lab-TekII chamber slides (Nalge Nunc International). In the case of siRNA experiments, 1.0×10^6 cells were electroporated, and plated on six-well plate dishes (Falcon). CGNs were incubated for the indicated period after addition of Ara-C (final 10 µM) at 24 h.

For cerebellar microexplant cultures, the cerebellum was dissected at P4-P6, and sagittal slices (150 µm) were subsequently prepared with a McIlwain tissue chopper (Mickle Laboratory Engineering). White matter and deep cerebellar nuclei were removed from the tissue slices. Rectangular pieces were then dissected from the remaining tissue, which mainly consisted of the EGL. The prepared rectangular microexplants were placed into DMEM supplemented with B27 on PDL-coated glass-bottomed dishes (MatTek) coated with laminin (Wako) and incubated for 3 days. The rectangular microexplants (from whole, medial and lateral cerebella) were also used for qPCR and immunoblotting analyses.

DNA microarray

Total RNA from the medial region of the *Rac1*$^{flox/flox}$;*Rac3*$^{-/-}$ and *Atoh1-Cre;Rac1*$^{flox/flox}$;*Rac3*$^{-/-}$ cerebella at P6 was extracted using TRIzol (Invitrogen). The quality and quantity of RNA were determined using the Agilent 2100 BioAnalyzer. Gene expression profiles were examined using the SurePrint G3 Mouse Gene Expression 8×60K Microarray kit (Agilent Technologies). The background-subtracted signal intensity of *Mid1* was normalized to that of the 75th percentile, *Actg1* (γ-actin) or *Tuba1a* (α-tubulin). The ratios of normalized *Mid1* signal (*Atoh1-Cre;Rac1*$^{flox/flox}$;*Rac3*$^{-/-}$/control) are presented.

Immunoprecipitation

Immunoprecipitation experiments to detect Rac1/MID1/mTOR complex were performed using HEK293 cells. For details, see the supplementary Materials and Methods.

Statistics

All data are presented as the mean±s.e.m. Details of measurements are included in the supplementary Materials and Methods. Two groups were compared using unpaired Student's *t*-tests or Kolmogorov–Smirnov test. For comparisons of more than two groups, one-way or two-way analyses of variance (ANOVA) were performed, followed by Bonferroni's post-hoc test of pairwise group differences. Statistical analyses were performed using Prism 6.0 software (GraphPad).

Acknowledgements

We thank Prof. Bernd Fritzsch (University of Iowa, USA) for providing *Atoh1-Cre* TG mice. We also thank Ms Aya Shimizu, MSc and Mr Isao Sakamoto, MPharm for their technical assistance.

Competing interests

The authors declare no competing or financial interests.

Author contributions

Conceptualization: T.U.; Methodology: T.U.; Formal analysis: T.N., T.U., Y.N.; Investigation: T.N., T.U., Y.N., H.S., N.C., Y. Hishikawa, H.K., M.K., E.K., Y. Hisa; Resources: H.K., M.S., I.d.C., A.A.; Data curation: T.U.; Writing - original draft: T.N., T.U.; Writing - review & editing: T.U.; Visualization: T.U.; Supervision: T.U., H.S., E.K., Y. Hisa, N.S.; Project administration: T.U., N.S.; Funding acquisition: T.U., N.S.

Funding

This work was supported by grants from the Japan Society for the Promotion of Science KAKENHI on Innovative Areas 'Fluorescence Live imaging' (to N.S.); the Japan Society for the Promotion of Science KAKENHI [17H04042 (to T.U.) and 17024038 (to A.A.)]; the Uehara Memorial Foundation (201320273 to T.U.); and the Hyogo Science and Technology Association (26087 to T.U.).

Data availability

DNA microarray data are available in the ArrayExpress database (www.ebi.ac.uk/arrayexpress) under accession number E-MTAB-5681.

Supplementary information

Supplementary information available online at
http://dev.biologists.org/lookup/doi/10.1242/dev.147900.supplemental

Development (2017) 144, 1863-1875 doi:10.1242/dev.147900

References

Akazawa, C., Ishibashi, M., Shimizu, C., Nakanishi, S. and Kageyama, R. (1995). A mammalian helix-loop-helix factor structurally related to the product of Drosophila proneural gene atonal is a positive transcriptional regulator expressed in the developing nervous system. *J. Biol. Chem.* **270**, 8730-8738.

Aranda-Orgillés, B., Trockenbacher, A., Winter, J., Aigner, J., Köhler, A., Jastrzebska, E., Stahl, J., Müller, E.-C., Otto, A., Wanker, E. E. et al. (2008). The Opitz syndrome gene product MID1 assembles a microtubule-associated ribonucleoprotein complex. *Hum. Genet.* **123**, 163-176.

Ayala, R., Shu, T. and Tsai, L.-H. (2007). Trekking across the brain: the journey of neuronal migration. *Cell* **128**, 29-43.

Basu, S. (2011). PP2A in the regulation of cell motility and invasion. *Curr. Protein Pept. Sci.* **12**, 3-11.

Ben-Arie, N., Bellen, H. J., Armstrong, D. L., McCall, A. E., Gordadze, P. R., Guo, Q., Matzuk, M. M. and Zoghbi, H. Y. (1997). Math1 is essential for genesis of cerebellar granule neurons. *Nature* **390**, 169-172.

Bosco, E. E., Mulloy, J. C. and Zheng, Y. (2009). Rac1 GTPase: a "Rac" of all trades. *Cell. Mol. Life Sci.* **66**, 370-374.

Chédotal, A. (2010). Should I stay or should I go? Becoming a granule cell. *Trends Neurosci.* **33**, 163-172.

Chen, L., Liao, G., Waclaw, R. R., Burns, K. A., Linquist, D., Campbell, K., Zheng, Y. and Kuan, C.-Y. (2007). Rac1 controls the formation of midline commissures and the competency of tangential migration in ventral telencephalic neurons. *J. Neurosci.* **27**, 3884-3893.

Chen, L., Melendez, J., Campbell, K., Kuan, C.-Y. and Zheng, Y. (2009). Rac1 deficiency in the forebrain results in neural progenitor reduction and microcephaly. *Dev. Biol.* **325**, 162-170.

Cloetta, D., Thomanetz, V., Baranek, C., Lustenberger, R. M., Lin, S., Oliveri, F., Atanasoski, S. and Ruegg, M. A. (2013). Inactivation of mTORC1 in the developing brain causes microcephaly and affects gliogenesis. *J. Neurosci.* **33**, 7799-7810.

Corbetta, S., Gualdoni, S., Albertinazzi, C., Paris, S., Croci, L., Consalez, G. G. and de Curtis, I. (2005). Generation and characterization of Rac3 knockout mice. *Mol. Cell. Biol.* **25**, 5763-5776.

Fontanella, B., Russolillo, G. and Meroni, G. (2008). MID1 mutations in patients with X-linked Opitz G/BBB syndrome. *Hum. Mutat.* **29**, 584-594.

Funahashi, Y., Namba, T., Nakamuta, S. and Kaibuchi, K. (2014). Neuronal polarization in vivo: Growing in a complex environment. *Curr. Opin. Neurobiol.* **27**, 215-223.

Govek, E.-E., Newey, S. E. and Van Aelst, L. (2005). The role of the Rho GTPases in neuronal development. *Genes Dev.* **19**, 1-49.

Graus-Porta, D., Blaess, S., Senften, M., Littlewood-Evans, A., Damsky, C., Huang, Z., Orban, P., Klein, R., Schittny, J. C. and Müller, U. (2001). Beta1-class integrins regulate the development of laminae and folia in the cerebral and cerebellar cortex. *Neuron* **31**, 367-379.

Gu, J., Sumida, Y., Sanzen, N. and Sekiguchi, K. (2001). Laminin-10/11 and fibronectin differentially regulate integrin-dependent Rho and Rac activation via p130(Cas)-CrkII-DOCK180 pathway. *J. Biol. Chem.* **276**, 27090-27097.

Gualdoni, S., Albertinazzi, C., Corbetta, S., Valtorta, F. and de Curtis, I. (2007). Normal levels of Rac1 are important for dendritic but not axonal development in hippocampal neurons. *Biol. Cell* **99**, 455-464.

Hatten, M. E., Alder, J., Zimmerman, K. and Heintz, N. (1997). Genes involved in cerebellar cell specification and differentiation. *Curr. Opin. Neurobiol.* **7**, 40-47.

Ishii, T., Ueyama, T., Shigyo, M., Kohta, M., Kondoh, T., Kuboyama, T., Uebi, T., Hamada, T., Gutmann, D. H., Aiba, A. et al. (2017). A novel Rac1-GSPT1 signaling pathway controls astrogliosis following central nervous system injury. *J. Biol. Chem.* **292**, 1240-1250.

Kassai, H., Terashima, T., Fukaya, M., Nakao, K., Sakahara, M., Watanabe, M. and Aiba, A. (2008). Rac1 in cortical projection neurons is selectively required for midline crossing of commissural axonal formation. *Eur. J. Neurosci.* **28**, 257-267.

Kawaji, K., Umeshima, H., Eiraku, M., Hirano, T. and Kengaku, M. (2004). Dual phases of migration of cerebellar granule cells guided by axonal and dendritic leading processes. *Mol. Cell. Neurosci.* **25**, 228-240.

Kawauchi, T., Chihama, K., Nabeshima, Y. and Hoshino, M. (2003). The in vivo roles of STEF/Tiam1, Rac1 and JNK in cortical neuronal migration. *EMBO J.* **22**, 4190-4201.

Komuro, H., Yacubova, E. and Rakic, P. (2001). Mode and tempo of tangential cell migration in the cerebellar external granular layer. *J. Neurosci.* **21**, 527-540.

Lancioni, A., Pizzo, M., Fontanella, B., Ferrentino, R., Napolitano, L. M. R., De Leonibus, E. and Meroni, G. (2010). Lack of Mid1, the mouse ortholog of the Opitz syndrome gene, causes abnormal development of the anterior cerebellar vermis. *J. Neurosci.* **30**, 2880-2887.

Laplante, M. and Sabatini, D. M. (2012). mTOR signaling in growth control and disease. *Cell* **149**, 274-293.

Liu, E., Knutzen, C. A., Krauss, S., Schweiger, S. and Chiang, G. G. (2011). Control of mTORC1 signaling by the Opitz syndrome protein MID1. *Proc. Natl. Acad. Sci. USA* **108**, 8680-8685.

Lu, T., Chen, R., Cox, T. C., Moldrich, R. X., Kurniawan, N., Tan, G., Perry, J. K., Ashworth, A., Bartlett, P. F., Xu, L. et al. (2013). X-linked microtubule-associated protein, Mid1, regulates axon development. *Proc. Natl. Acad. Sci. USA* **110**, 19131-19136.

Matei, V., Pauley, S., Kaing, S., Rowitch, D., Beisel, K. W., Morris, K., Feng, F., Jones, K., Lee, J. and Fritzsch, B. (2005). Smaller inner ear sensory epithelia in Neurog1 null mice are related to earlier hair cell cycle exit. *Dev. Dyn.* **234**, 633-650.

Montalvo-Ortiz, B. L., Castillo-Pichardo, L., Hernández, E., Humphries-Bickley, T., De la Mota-Peynado, A., Cubano, L. A., Vlaar, C. P. and Dharmawardhane, S. (2012). Characterization of EHop-016, novel small molecule inhibitor of Rac GTPase. *J. Biol. Chem.* **287**, 13228-13238.

Mulherkar, S., Uddin, M. D., Couvillon, A. D., Sillitoe, R. V. and Tolias, K. F. (2014). The small GTPases RhoA and Rac1 regulate cerebellar development by controlling cell morphogenesis, migration and foliation. *Dev. Biol.* **394**, 39-53.

Nagata, I. and Nakatsuji, N. (1990). Granule cell behavior on laminin in cerebellar microexplant cultures. *Brain Res. Dev. Brain Res.* **52**, 63-73.

Nanahoshi, M., Nishiuma, T., Tsujishita, Y., Hara, K., Inui, S., Sakaguchi, N. and Yonezawa, K. (1998). Regulation of protein phosphatase 2A catalytic activity by alpha4 protein and its yeast homolog Tap42. *Biochem. Biophys. Res. Commun.* **251**, 520-526.

Pinson, L., Auge, J., Audollent, S., Mattei, G., Etchevers, H., Gigarel, N., Razavi, F., Lacombe, D., Odent, S., Le Merrer, M. et al. (2004). Embryonic expression of the human MID1 gene and its mutations in Opitz syndrome. *J. Med. Genet.* **41**, 381-386.

Quevedo, C., Sauzeau, V., Menacho-Marquez, M., Castro-Castro, A. and Bustelo, X. R. (2010). Vav3-deficient mice exhibit a transient delay in cerebellar development. *Mol. Biol. Cell* **21**, 1125-1139.

Saci, A., Cantley, L. C. and Carpenter, C. L. (2011). Rac1 regulates the activity of mTORC1 and mTORC2 and controls cellular size. *Mol. Cell* **42**, 50-61.

Sakai, K., Hasegawa, C., Okura, M., Morikawa, O., Ueyama, T., Shirai, Y., Sakai, N. and Saito, N. (2003). Novel variants of murine serotonin transporter mRNA and the promoter activity of its upstream site. *Neurosci. Lett.* **342**, 175-178.

Sanchez, C., Diaz-Nido, J. and Avila, J. (2000). Phosphorylation of microtubule-associated protein 2 (MAP2) and its relevance for the regulation of the neuronal cytoskeleton function. *Prog. Neurobiol.* **61**, 133-168.

Schweiger, S. and Schneider, R. (2003). The MID1/PP2A complex: a key to the pathogenesis of Opitz BBB/G syndrome. *BioEssays* **25**, 356-366.

Sgaier, S. K., Millet, S., Villanueva, M. P., Berenshteyn, F., Song, C. and Joyner, A. L. (2005). Morphogenetic and cellular movements that shape the mouse cerebellum; insights from genetic fate mapping. *Neuron* **45**, 27-40.

Short, K. M., Hopwood, B., Yi, Z. and Cox, T. C. (2002). MID1 and MID2 homo- and heterodimerise to tether the rapamycin-sensitive PP2A regulatory subunit, alpha 4, to microtubules: implications for the clinical variability of X-linked Opitz GBBB syndrome and other developmental disorders. *BMC Cell Biol.* **3**, 1.

Stankiewicz, T. R. and Linseman, D. A. (2014). Rho family GTPases: key players in neuronal development, neuronal survival, and neurodegeneration. *Front. Cell. Neurosci.* **8**, 314.

Stankiewicz, T. R., Ramaswami, S. A., Bouchard, R. J., Aktories, K. and Linseman, D. A. (2015). Neuronal apoptosis induced by selective inhibition of Rac GTPase versus global suppression of Rho family GTPases is mediated by alterations in distinct mitogen-activated protein kinase signaling cascades. *J. Biol. Chem.* **290**, 9363-9376.

Tahirovic, S., Hellal, F., Neukirchen, D., Hindges, R., Garvalov, B. K., Flynn, K. C., Stradal, T. E., Chrostek-Grashoff, A., Brakebusch, C. and Bradke, F. (2010). Rac1 regulates neuronal polarization through the WAVE complex. *J. Neurosci.* **30**, 6930-6943.

Takei, N., Inamura, N., Kawamura, M., Namba, H., Hara, K., Yonezawa, K. and Nawa, H. (2004). Brain-derived neurotrophic factor induces mammalian target of rapamycin-dependent local activation of translation machinery and protein synthesis in neuronal dendrites. *J. Neurosci.* **24**, 9760-9769.

Thomanetz, V., Angliker, N., Cloëtta, D., Lustenberger, R. M., Schweighauser, M., Oliveri, F., Suzuki, N. and Rüegg, M. A. (2013). Ablation of the mTORC2 component rictor in brain or Purkinje cells affects size and neuron morphology. *J. Cell Biol.* **201**, 293-308.

Trockenbacher, A., Suckow, V., Foerster, J., Winter, J., Krauß, S., Ropers, H.-H., Schneider, R. and Schweiger, S. (2001). MID1, mutated in Opitz syndrome, encodes an ubiquitin ligase that targets phosphatase 2A for degradation. *Nat. Genet.* **29**, 287-294.

Ueyama, T., Geiszt, M. and Leto, T. L. (2006). Involvement of Rac1 in activation of multicomponent Nox1- and Nox3-based NADPH oxidases. *Mol. Cell. Biol.* **26**, 2160-2174.

Ueyama, T., Sakaguchi, H., Nakamura, T., Goto, A., Morioka, S., Shimizu, A., Nakao, K., Hishikawa, Y., Ninoyu, Y., Kassai, H. et al. (2014). Maintenance of stereocilia and apical junctional complexes by Cdc42 in cochlear hair cells. *J. Cell Sci.* **127**, 2040-2052.

Ueyama, T., Ninoyu, Y., Nishio, S.-Y., Miyoshi, T., Torii, H., Nishimura, K., Sugahara, K., Sakata, H., Thumkeo, D., Sakaguchi, H. et al. (2016).

Development (2017) 144, 1863-1875 doi:10.1242/dev.147900

Constitutive activation of DIA1 (DIAPH1) via C-terminal truncation causes human sensorineural hearing loss. *EMBO Mol. Med.* **8**, 1310-1324.

Wang, V. Y. and Zoghbi, H. Y. (2001). Genetic regulation of cerebellar development. *Nat. Rev. Neurosci.* **2**, 484-491.

Wang, V. Y., Rose, M. F. and Zoghbi, H. Y. (2005). Math1 expression redefines the rhombic lip derivatives and reveals novel lineages within the brainstem and cerebellum. *Neuron* **48**, 31-43.

Yamasaki, T., Kawaji, K., Ono, K., Bito, H., Hirano, T., Osumi, N. and Kengaku, M. (2001). Pax6 regulates granule cell polarization during parallel fiber formation in the developing cerebellum. *Development* **128**, 3133-3144.

Yoshizawa, M., Kawauchi, T., Sone, M., Nishimura, Y. V., Terao, M., Chihama, K., Nabeshima, Y.-I. and Hoshino, M. (2005). Involvement of a Rac activator, P-Rex1, in neurotrophin-derived signaling and neuronal migration. *J. Neurosci.* **25**, 4406-4419.

Supplementary Information

Supplementary Materials and Methods

Animals and genotyping of animals

The animal experiments were conducted in accordance with the guidelines of Kobe University. Both males and females were used in the analyses because the phenotypes of *Atoh1-Cre;Rac1*$^{flox/flox}$*;Rac3*$^{-/-}$ mice did not exhibit significant differences between the sexes. Experimental groups with mice older than 4 weeks were organized according to sex. Offspring were genotyped via PCR using the following primer pairs for *Atoh1-Cre* (5′-GCATACCTGGAAAATGCTTC-3′ and 5′-CCAGTGAAACAGCATTGCTG-3′), *Rac1*^{flox} (5′-ATTTTCTAGATTCCACTTGTGAAC-3′ and 5′-ATCCCTACTTCCTTCCAACTC-3′), *Rac3*$^{-}$ (5′-CATTTCTGTGGCGTCGCCAAC-3′ and 5′-TTGCTGGTGTCCAGACCAAT-3′), *Rac3*$^{+}$ (5′-CATTTCTGTGGCGTCGCCAAC-3′ and 5′-CACGCGGCCGAGCTGTGGTG-3′), and *tdTomato* (5′-GGCATTAAAGCAGCGTATCC-3′ and 5′-CTGTTCCTGTACGGCATGG-3′). The obtained *Atoh1-Cre;tdTomato* mice were used to examine the effect of the Atoh1 promoter, while *Atoh1-Cre;Rac1*$^{flox/flox}$*;Rac3*$^{-/-}$*;tdTomato* mice were used to identify CGNs and evaluate vertical neurites of CGNs *in vivo*. Wildtype (WT; C57BL/6) mice were purchased from Clea Japan.

Cells and antibodies

RN46A, PC12, and HEK293 (ATCC) cells were maintained in DMEM/Ham's F12 medium (Wako Pure Chemical Industries) containing 10% FBS (Nichirei Biosciences), DMEM (Wako) containing 10% FBS and 5% horse serum (Invitrogen), and EMEM (Wako) containing 10% FBS and 100 μM nonessential amino acids (Wako), respectively.

The following specific antibodies (Abs) were used for immunoblotting (monoclonal

unless indicated): Rac1 (23A8) (Millipore, 1/1000); S6 ribosomal protein (5G10), phospho-S6 ribosomal protein(Ser240/244) (D68F8), 4E-BP1 polyclonal, and phospho-4E-BP1(Thr37/46) (236B4) (Cell Signaling Technology, 1/1000); MID1 polyclonal (A302-227A, Bethyl Laboratories, 1/500), which recognizes endogenous human MID1 but not endogenous mouse or rat Mid1; and MID1 polyclonal (ab70770, Abcam, 1/1000), which recognizes endogenous mouse Mid1; PP2A catalytic α (610555, BD Biosciences, 1/1000).

The following specific Abs were used for immunohistochemistry: calbindin polyclonal (AB1778, Millipore, 1/1000); Pax6 polyclonal (PD022, MBL international, 1/200); $p27^{Kip1}$ (610241, BD Biosciences, 1/100); NeuN (A60) (Millipore, 1/100); cleaved Caspase-3(Asp175) polyclonal (1/1000), MAP2 (M3696, Sigma-Aldrich, 1/100); neuron specific βIII tubulin (Tuj1) (MMS-435P, Covance, 1/500); Tuj1 polyclonal (ab18207, Abcam, 1/1000); and a red fluorescent protein (RFP) polyclonal Ab, whose reactivity to tdTomato has been certified (PM005, MBL International, 1/200). HRP-conjugated GAPDH or tubulin-α Abs were obtained from MBL International. Alexa488 (or 568)-conjugated secondary Abs (1/2000) were obtained from Invitrogen.

Plasmids and RNA interference

Mouse *Mid1* cDNA and human *MID1* cDNA were obtained from RIKEN (Japan) and cloned into p3×FLAG-CMV-10 (Sigma-Aldrich). We utilized an Myc-tagged human Rac1 plasmid and a validated RNAi sequence for rat/mouse/human *RAC1* that have been previously described (Ueyama et al., 2006). The siRNAs for *RAC1* (siRac1), rat/mouse *Mid1* (siMid1-832: 5′-CAAATTATTGGAACAAAG-3′; siMid1-1107: 5′-GAAGAAACTGCTAGAATGT-3′), and control siRNA (MISSION Universal Negative Control) were purchased from Sigma-Aldrich. Different types of siRNAs for rat *Mid1* and controls (SMARTpool and Non-targeting pool) were purchased from Thermo Fisher

Scientific. The siRNAs were transfected into neuronal cells (RN46A, PC12, and mouse/rat primary CGNs) and HEK293 cells using a NEPA21 electroporator (NEPA GENE Co., Ltd.) and Lipofectamine 3000 (Invitrogen), respectively, and the cells were used for experiments 48 h after transfection. Compared with lipofection, electroporation has been reported to require a higher concentration of siRNAs (Ovcharenko et al., 2005); thus, 5–40 nM of siRNAs were used for electroporation.

Immunoblotting

Cells and dissected cerebellar cortexes were lysed in homogenizing buffer (Ueyama et al., 2016) in the presence of protease inhibitor cocktail, protein phosphatase inhibitor cocktail (Nacalai Tesque), and 1% Triton X-100. Total lysates were centrifuged at 12,000 × *g* for 20 min at 4°C, and the supernatants were subjected to SDS–PAGE, followed by immunoblotting for 2 h at 25°C using primary Abs. The bound primary Abs were detected using the ECL detection system (Bio-Rad Laboratories). For quantification, the relative levels of protein and phosphorylated protein expression were normalized to those of α-tubulin and total target protein, respectively.

ISH

ISH was performed using the following forty-five-base pair DNA probes labeled at their 5′-end with digoxigenin-11-dUTP: for mouse *Rac1* (antisense [nucleotides 346–390 from ATG]: 5′-GAGCAGGCAGGTTTTACCAACAGCTCCGTCTCCCACCACCACACA-3′ and sense: 5′-TGTGTGGTGGTGGGAGACGGAGCTGTTGGTAAAACCTGCCTGCTC-3′), for mouse *Rac3* (antisense [155–199]: 5′-CAGCAGGCACGTCTTCCCCACGGCACCATCGCCAACCACCACGCA-3′ and sense: 5′-TGCGTGGTGGTTGGCGATGGTGCCGTGGGGAAGACGTGCCTGCTG-3′),

and for mouse *Mid1* (antisense [125–169]: 5′-GGCACTGGAAGGCGTTGATGGACTCCACAGGCTCGTTGGTGGCAC-3′ and sense: 5′-GTGCCACCAACGAGCCTGTGGAGTCCATCAACGCCTTCCAGTGCC-3′). ISH signals were detected immunohistochemically. The staining intensities of sense and antisense probes were compared using a digital image analyzer (Winroof version 7.0, Mitani Corp).

qPCR

The following primer pairs were used for rat *Mid1* cDNA (SET1: 5′-TCCAAAAAGAGTCACACACC-3′ and 5′-TAAACACATTTCCAGCCACG-3′, SET2: 5′-GTGGTGAGACATAACAGCAAAG-3′ and 5′-CGAAGGTATAGAGGTGGATGG-3′), mouse *Mid1* cDNA (5′-AGAGAAACACAGAACTGGAGACT-3′ and 5′-CAGTTTGGCTTCTTGACGGG-3′), rat *Actb* cDNA (5′-CGTGAAAAGATGACCCAGATCA-3′ and 5′-CTCCGGAGTCCATCACAATG-3′), rat *Gapdh* cDNA (5′-CTGCACCACCAACTGCTTAG-3′ and 5′-TGATGGCATGGACTGTGG-3′), and mouse *Gapdh* cDNA (5′-TGCACCACCAACTGCTTAGC-3′ and 5′-GGATGCAGGGATGATGTTCT-3′). Gene expression was normalized to the expression of *Actb* or *Gapdh* as an internal control gene. The $\Delta\Delta C_T$ method (Livak and Schmittgen, 2001) was applied as a comparative quantification method. The specificity of the amplified fragment was demonstrated by the melting curve with a single peak.

RT-PCR

The following primer pairs were used for PCR of mouse *Rac1* cDNA (5′-GCAGACAGACGTGTTCTTAATTTGC-3′ and 5′-TGTAACAAAAACTTGGCATCAAATGCG-3′) and mouse *Rac3* cDNA

(5′-CCAGGAAGACTACGATAGGCTT-3′ and 5′-TGGAGCTATATCCCAGAAAAAGGAG-3′).

Immunoprecipitation

FLAG-tagged MID1 + Myc-tagged Rac1 or HA-tagged mTOR + FLAG-tagged MID1 + Myc-tagged Rac1 was transfected into HEK293 cells plated on 10-cm dish using FuGENE6 (Promega). Forty-eight hours after transfection, the cells were lysed in 250 µl in lysis buffer (25 mM Tris-HCl; pH 8.0, 150 mM NaCl, 10 mM $MgCl_2$, 1 mM EDTA, 0.25% NP40) by sonication. The total cell lysates were centrifuged at 12,000 ×*g* for 20 min at 4°C, and the supernatants were rotated with 10 µl of magnetic beads (MB)-conjugated Myc mAb (PL14, MBL International), MB-conjugated HA mAb (TANA2, MBL International), or control MB (MBL International) for 2 h at 4°C. The precipitates were washed three times using a magnetic rack with the buffer, the material absorbed to beads was eluted in the Laemmli's sample buffer, and the magnetic beads were removed using magnetic rack. The aliquots of elutants were subjected to SDS-PAGE followed by immunoblotting using a Myc mAb (MBL International) and FLAG mAb (MBL International) with or without mTOR mAb (Cell Signaling Technology).

Measurements

Tangential migration of CGNs at E16.5 was defined as the curvature distance from the upper rim of the RL to the anterior-most edge of the EGL in four sagittal sections (Fig. 3A).

The total neurite length/field of primary CGNs was defined as the sum of the lengths of all βIII tubulin-immunopositive neurites. Neurite length in the microexplant was defined as the length from the edge of the microexplant to the leading edge of the longest βIII tubulin-immunopositive neurite (Fig. 8B).

The migration (tangential) of CGNs in cerebellar microexplants was defined as the

distance from the edge of the microexplant to the nucleus of migrated CGNs. In each microexplant, the migrated CGNs resided in a 200-μm-wide rectangle that included the farthest CGNs that were analyzed (Fig. S3A; total of >2200 CGNs of 17 microexplants from six mice).

For KD experiments using microexplants, microexplants were placed on PDL-coated glass-bottom dishes coated with laminin in DMEM supplemented with B27. The siRNAs were then transfected into the microexplants using Lipofectamine RNAiMAX (Invitrogen). Seven hours after transfection, the culture medium was replaced with DMEM supplemented with B27. Cells with green fluorescence (BLOCK-iT:FITC, Invitrogen) were recognized as siRNA-transfected cells, and the migration of CGNs was analyzed 60 h after transfection (Fig. S5; 486 control CGNs of 29 microexplants, and 339 Mid1-KD CGNs of 35 microexplants from three independent experiments).

The siRNA and pEGFP plasmids were co-electroporated into primary CGNs, and EGFP-expressing cells were recognized as siRNA-transfected cells. The longest neurite length in 20 primary CGNs for each experiment (total 60 neurons) was quantified (Fig. 10C, D). All these parameters were measured using ImageJ software (National Institutes of Health) in at least three independent experiments.

References

Livak, K. J. and Schmittgen, T. D. (2001). Analysis of relative gene expression data using real-time quantitative PCR and the 2(-Delta Delta C(T)) Method. *Methods* **25**, 402-8.
Ovcharenko, D., Jarvis, R., Hunicke-Smith, S., Kelnar, K. and Brown, D. (2005). High-throughput RNAi screening in vitro: from cell lines to primary cells. *RNA* **11**, 985-93.
Ueyama, T., Geiszt, M. and Leto, T. L. (2006). Involvement of Rac1 in activation of multicomponent Nox1- and Nox3-based NADPH oxidases. *Molecular and cellular biology* **26**, 2160-74.
Ueyama, T., Ninoyu, Y., Nishio, S. Y., Miyoshi, T., Torii, H., Nishimura, K., Sugahara, K., Sakata, H., Thumkeo, D., Sakaguchi, H. et al. (2016). Constitutive activation of DIA1 (DIAPH1) via C-terminal truncation causes human sensorineural hearing loss. *EMBO Mol Med* **8**, 1310-1324.

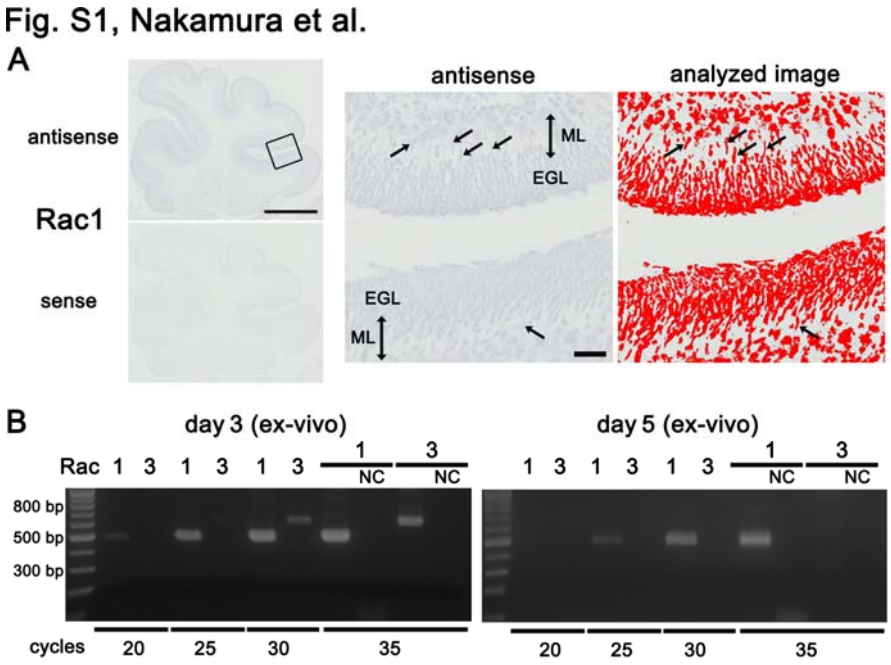

Fig. S1: Migrating slender cells in the ML are *Rac1*-positive, and *Rac1* is predominantly expressed in CGNs. (**A**) ISH of *Rac1* was performed using P6 sagittal sections of the cerebellum with antisense and sense DNA probes. The rectangle shows the location of the magnified panel (scale bars: 500 µm, 25 µm in the magnified panel). The arrows indicate migrating slender cells expressing *Rac1* mRNA in the molecular layer (ML). The right panel shows the relative *Rac1* mRNA signal level determined by a digital image analyzer (red was assigned to positive). EGL: external granule layer. n≥4 for each group. (**B**) RT was performed with 1 µg of total RNA obtained from WT mouse primary CGNs cultured for 3 days (left) or 5 days (right). Mouse *Rac1* and *Rac3* cDNAs were amplified by PCR: the PCR cycle number was 20, 25, 30, and 35. On day 3, *Rac1* and *Rac3* bands were observed from 20 cycles and 30 cycles, respectively. On day 5, *Rac1* band was observed from 25 cycles but *Rac3* band is not observed. NC: negative control. n=3.

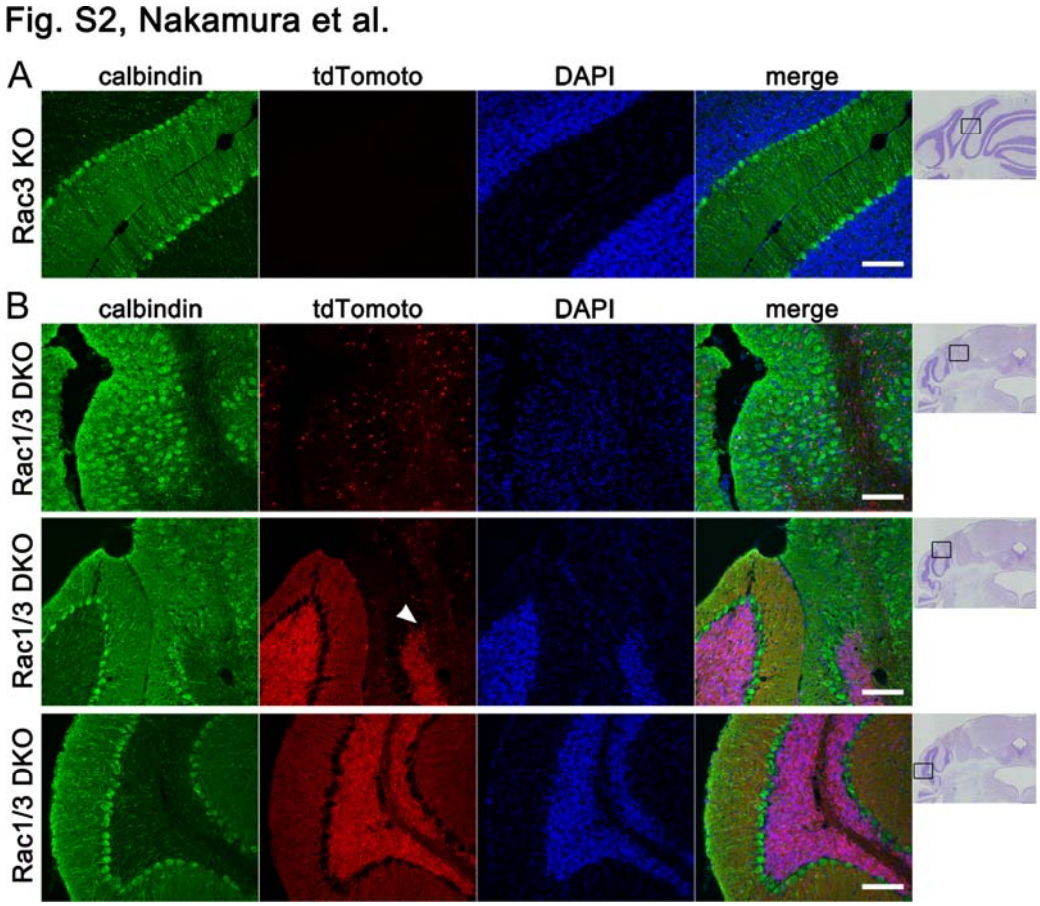

Fig. S2: Aberrant localization of PCs in the medial *Atoh1-Cre;Rac1$^{flox/flox}$;Rac3$^{-/-}$* cerebellum. *Rac1$^{flox/flox}$;Rac3$^{-/-}$;tdTomato* (*Rac3* KO) and *Atoh1-Cre;Rac1$^{flox/flox}$;Rac3$^{-/-}$;tdTomato* (*Rac1/Rac3* DKO) mice were fixed at 12 weeks of age. Coronal sections of the *Rac*3-KO (**A**) and *Rac1/Rac3*-DKO cerebellum (**B**: upper panels, medial cerebellum; bottom panels, lateral cerebellum; middle panels, border region between the medial and lateral cerebellum) were stained using a calbindin Ab with DAPI. In the *Rac*3-KO and the lateral *Rac1/Rac3*-DKO cerebellum, a single layer of calbindin-positive Purkinje cells (PCs) is observed. In the lateral *Rac1/Rac3*-DKO cerebellum, an internal granule layer (IGL) consisting of tdTomato-positive cerebellar granule neurons (CGNs) is also observed. In sharp contrast, the medial *Rac1/Rac3*-DKO cerebellum exhibits multiple layers of calbindin-positive PCs and diffusely localized tdTomato-positive CGNs in the affected regions. In the border region between the medial and lateral cerebellum (middle panels in B), an IGL consisted of tdTomato-positive CGNs is tapered (arrowhead). Medial to this border, tdTomato-positive CGNs are sparsely localized in multiple layers of calbindin-positive PCs. The rectangles in the low-magnification images of the coronal sections (most right) indicate the location of the cerebellum depicted in the corresponding high-magnification images. Scale bars: 100 μm. n =3.

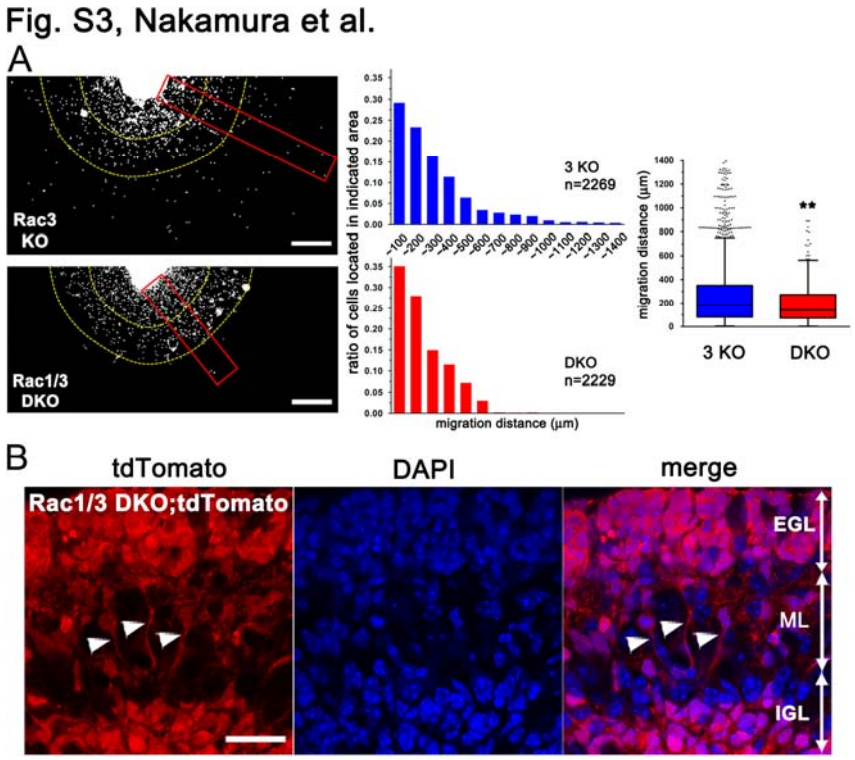

Fig. S3: Impaired migration in *Atoh1-Cre;Rac1$^{flox/flox}$;Rac3$^{-/-}$* cerebellar microexplants and normal development of vertical neurites of CGNs in the posterior lobe of *Atoh1-Cre;Rac1$^{flox/flox}$;Rac3$^{-/-}$;tdTomato* cerebellum. (**A**) After 3 days in culture, cerebellar microexplants from *Rac1$^{flox/flox}$;Rac3$^{-/-}$* (*Rac3* KO) and *Atoh1-Cre;Rac1$^{flox/flox}$;Rac3$^{-/-}$* (*Rac1/Rac3* DKO) mice were fixed and stained using DAPI. The migration distance from the microexplant (DAPI-positive cells are shown by white dots, n > 2200 CGNs from 17 microexplants) was quantified (***P*< 0.01 using the Kolmogorov–Smirnov test). The ratio of the number of cells residing in every 100-µm bin/number of total cells in a 200-µm rectangle was calculated and graphed. The lower and higher whiskers in the boxplots indicate the lowest and highest data, respectively, within 1.5 interquartile ranges of the respective quartiles. Outliers are represented by circles. The yellow, dotted circular lines indicate 300 µm and 600 µm from the microexplant. The red 200-µm-wide rectangles show the areas analyzed in these samples. Scale bars: 300 µm. (**B**) At P8, *Atoh1-Cre;Rac1$^{flox/flox}$;Rac3$^{-/-}$;tdTomato* (*Rac1/Rac3* DKO) mice were fixed. Sagittal sections were stained using an RFP Ab with DAPI. Arrowheads indicate tdTomato-positive vertical neurites inwardly projecting from radially migrating CGNs in the posterior lobe. ML: molecular layer. Scale bars: 25 µm. n=3.

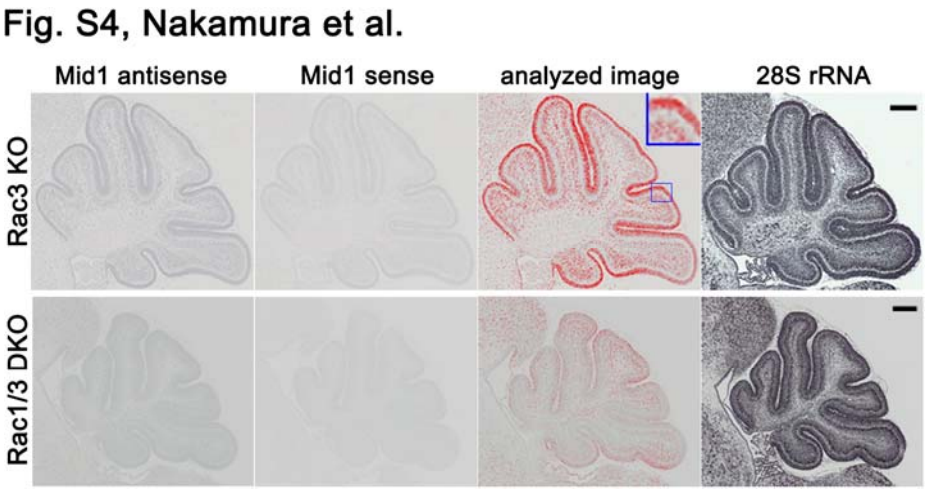

Fig. S4: Selective expression of *Mid1* mRNA in the EGL. Sagittal sections of the cerebellum were obtained from *Rac1*$^{flox/flox}$;*Rac3*$^{-/-}$ (*Rac3* KO) and *Atoh1-Cre;Rac1*$^{flox/flox}$;*Rac3*$^{-/-}$ (*Rac1/Rac3* DKO) mice at P5. ISH of *Mid1* was performed using antisense and sense DNA probes labeled with digoxigenin-11-dUTP. The relative *Mid1* mRNA signal levels were determined using a digital image analyzer (red was assigned to positive). The EGL of *Rac3*-KO mice was selectively positive for *Mid1*, the expression of which was significantly decreased in *Rac1/Rac3*-DKO mice. The inset contains a magnified image of the area indicated by the rectangle. Scale bars: 500 μm. n=3.

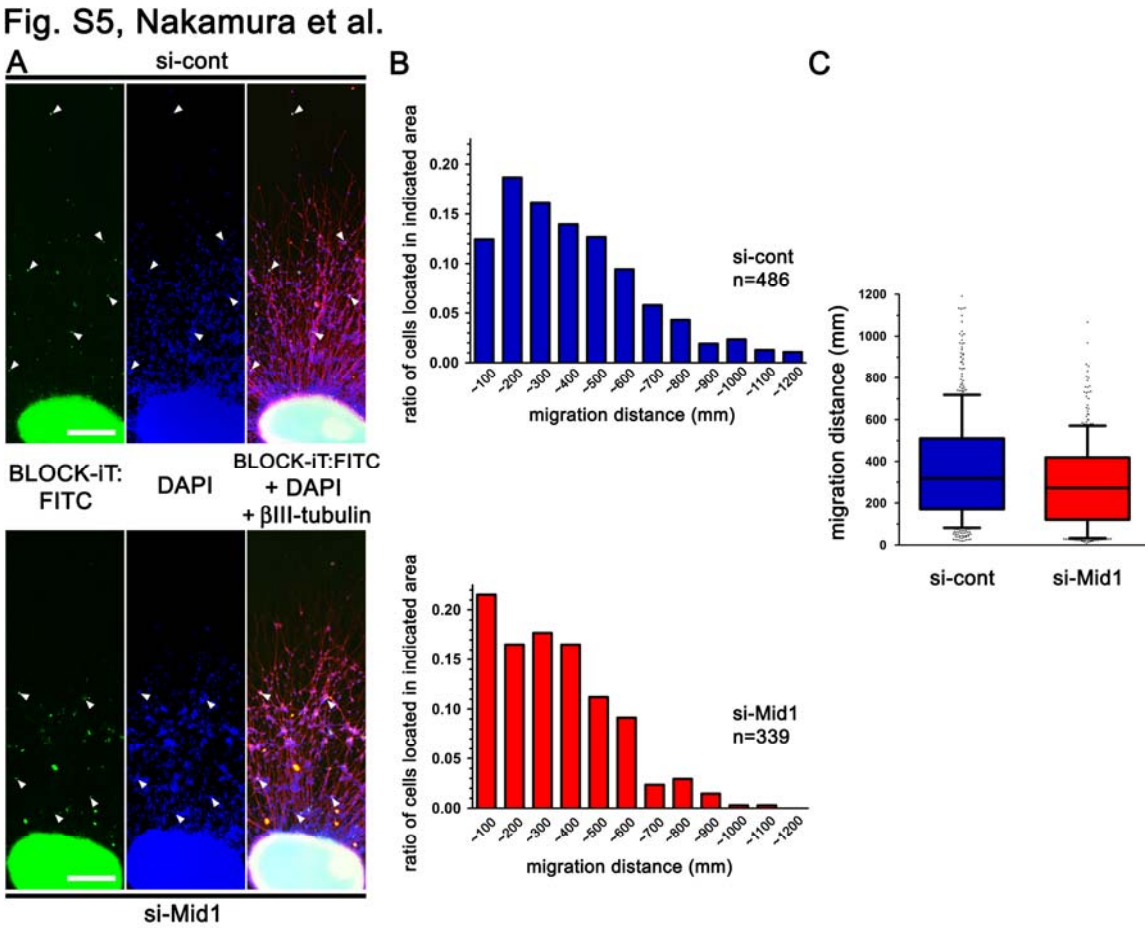

Fig. S5: Impaired migration of *Mid1*-KD CGNs in cerebellar microexplants. (**A**) We transfected siRNA (si-cont or siMid1-832 [7.5 nM] + 12.5 nM BLOCK-iT fluorescent oligo [BLOCK-iT:FITC]) into microexplants using Lipofectamine RNAiMAX for 7 h in DMEM supplemented with B27. Sixty hours after transfection, samples were fixed and stained with βIII-tubulin + DAPI, and cell migration was analyzed. Cells with green fluorescence (arrowheads) were recognized as siRNA-transfected cells. (**B**) The ratio of the number of transfected cells residing in every 100-μm bin/number of total transfected cells migrated from explants was calculated and graphed (486 control CGNs of 29 explants and 339 *Mid1*-KD CGNs of 35 explants from three independent experiments). (**C**) The migration distance from the microexplant of siRNA-transfected cells were quantified (***P*< 0.01 by the Kolmogorov–Smirnov test). The lower and higher whiskers in the boxplots indicate the lowest and highest data, respectively, within 1.5 interquartile ranges of the respective quartiles. Outliers are represented by circles. Scale bars: 200 μm.

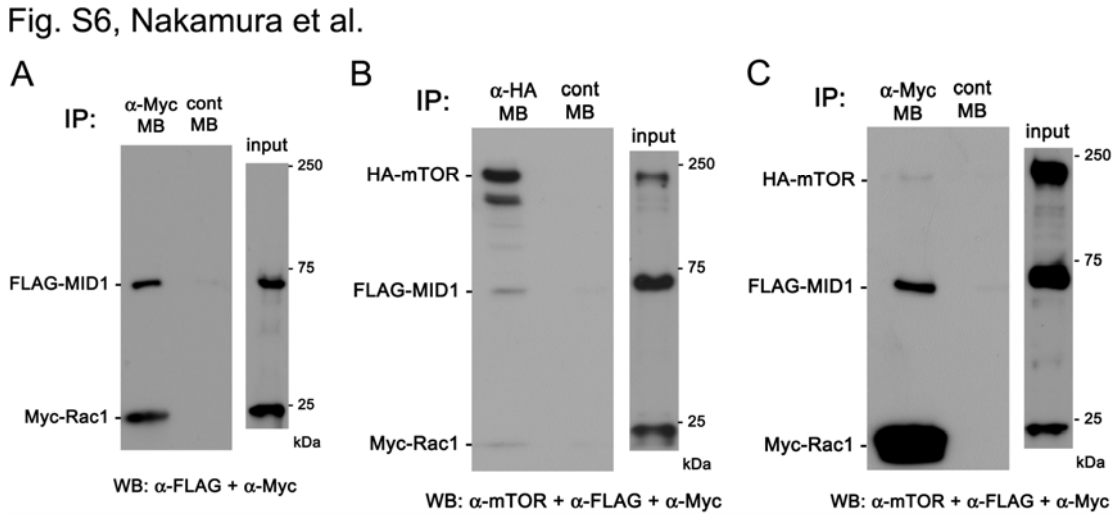

Fig. S6: Interactions of Rac1, MID1, and mTOR (Rac1/MID1/mTOR complex). FLAG-tagged MID1 + Myc-tagged Rac1 (**A**) or HA-tagged mTOR + FLAG-tagged MID1 + Myc-tagged Rac1 (**B** and **C**) was transfected into HEK293 cells. Forty-eight hours after transfection, supernatants of cell lysates were rotated with magnetic beads (MB)-conjugated Myc mAb (**A** and **C**), MB-conjugated HA mAb (**B**), and control MB (**A**-**C**). The material absorbed to MB was subjected to SDS-PAGE followed by immunoblotting using FLAG mAb + Myc mAb (**A**) or mTOR mAb + FLAG mAb + Myc mAb (**B** and **C**). MID1 is immunoprecipitated with Rac1 (**A**), MID1 and Rac1 are immunoprecipitated with mTOR (**B**), and mTOR and MID1 are immunoprecipitated with Rac1 (**C**). n=3

Movie 1

Ataxic gait of 9-week-old *Atoh1-Cre;Rac1*$^{flox/flox}$*;Rac3*$^{-/-}$ (*Rac1/Rac3* DKO) mouse.